Chapter 10

COMPRESSOR STAGE AERODYNAMIC DESIGN

The aerodynamic design of an axial-flow compressor stage involves definition of the rotor and stator velocity triangles and blade geometry that will produce desired stage performance characteristics. When appropriate, this may include the design of inlet and exit guide vanes as well. In the context used in this book, there are subtle but important differences between stage design and compressor design. Stage design will involve the selection of basic dimensionless performance parameters and the design of appropriate blade rows to produce them. No specific reference is made to the precise application of the stage in an actual compressor. Without knowledge of the specific working fluid, Mach number levels, matching with adjacent stages, etc., stage design is a rather idealized process. It is not possible to establish precise end-wall contours and compute the losses in this context. The purpose of this chapter is to introduce basic dimensionless performance parameters and to discuss their application to the design process. Representative applications of the stage designs will be used to indicate some of the consequences of the choices made. Chapter 11 extends these basic design concepts to the design of blade rows for complete axial-flow compressors with specific operating conditions and working fluids.

The stage-design procedures described in this chapter offer far more than abstract educational value. They certainly can be used to design stages for actual applications within a compressor, although the procedures in chapter 11 are more efficient. They often play a key role in the design of industrial axial-flow compressors. Each industrial axial-flow compressor usually has a unique design. Development and manufacturing costs become primary considerations when there are no duplicate machines to share them. It is fairly common practice to employ a standard repeating stage design for these compressors. Blade stagger angles are commonly adjusted to accommodate the specific applications. Scaling of the blades with corresponding modification of the number of blades per row may be used to satisfy mechanical strength requirements. Since the precise application is not predefined and unique designs for all stages are not acceptable, the design of a standard repeating stage will precisely follow the process described in this chapter. The specific axial-flow compressor design will involve application of this standard stage design with appropriate sizing of the annulus and various minor adjustments to accommodate the application. An example of this use of stage design procedures is included at the end of this chapter.

NOMENCLATURE

C = absolute velocity
c = chord
H = total enthalpy
h = static enthalpy
i = incidence angle
K = ψ / ψ_{lim}
m = vortex exponent
n = vortex exponent
P = pressure
P_R = pressure ratio
R = reaction
R_R = recovery ratio
r = radius
t_b = maximum blade thickness
U = local blade speed = ωr
W = relative velocity
Z = number of blades
z = axial coordinate
β = flow angle
γ = stagger angle
δ = deviation angle
η = efficiency
θ = camber angle
κ = blade camberline angle
ρ = gas density
σ = solidity
ϕ = flow coefficient
ψ = work coefficient
ψ_{lim} = value of ψ yielding $W_2 / W_1 = 0.7$
ω = rotation speed, radians/sec.

Subscripts

c = parameter on the reference radius
h = hub condition
R = rotor parameter
S = stator parameter
s = shroud condition
t = total thermodynamic condition
z = axial component
θ = tangential component
0 = inlet guide vane inlet condition
1 = rotor inlet condition
2 = stator inlet condition
3 = stator exit condition
4 = exit guide vane exit condition

Superscripts

* = minimum loss condition
′ = relative condition

10.1 DIMENSIONLESS PERFORMANCE PARAMETERS

In the design of an axial-flow compressor stage, the designer normally wants to control the flow capacity, the work done per stage and the distribution of the flow diffusion load between the rotor and stator. The specifications should be dimensionless to enable application to any specific stage inlet thermodynamic conditions, rotation speed and geometrical scale. This leads quite naturally to the dimensionless performance parameters introduced in Chapter 1, Section 1.5. If ω is the rotation speed, the local blade speed is given by $U = \omega r$. The dimensionless flow capacity of the stage will be governed by the dimensionless axial velocity component or flow coefficient, defined by

$$\phi = C_{z1} / U \tag{10-1}$$

The flow coefficient has been defined at the rotor inlet, since an inlet guide vane is not necessarily defined as part of the stage design process. The dimensionless work per stage follows directly from the Euler turbine equation, Eq. (3-9). The work coefficient is defined as

$$\psi = (H_2 - H_1) / U^2 = (C_{\theta 2} - C_{\theta 1}) / U \tag{10-2}$$

where the subscripts 1 and 2 refer to the rotor inlet and exit stations, respectively, using the station nomenclature illustrated in Fig. 10-1. The distribution of the flow diffusion between the rotor and stator can be expressed in terms of the fraction of the stage static enthalpy rise that occurs in the rotor, i.e., the stage reaction, defined as

$$R = (h_2 - h_1) / (h_3 - h_1) \tag{10-3}$$

Alternatively, reaction may be defined in terms of static pressures, but that is less convenient for the design problem. Since $C_r = 0$ for this case, Eq. (3-11) and the basic kinematics of the velocity components yield,

$$H = h + \tfrac{1}{2} C^2 \tag{10-4}$$

$$C^2 = C_z^2 + C_\theta^2 \tag{10-5}$$

Noting that $H_3 = H_2$, Eqs. (10-2) and (10-4) yield

$$h_2 - h_1 = U(C_{\theta 2} - C_{\theta 1}) - (C_2^2 - C_1^2) / 2 \tag{10-6}$$

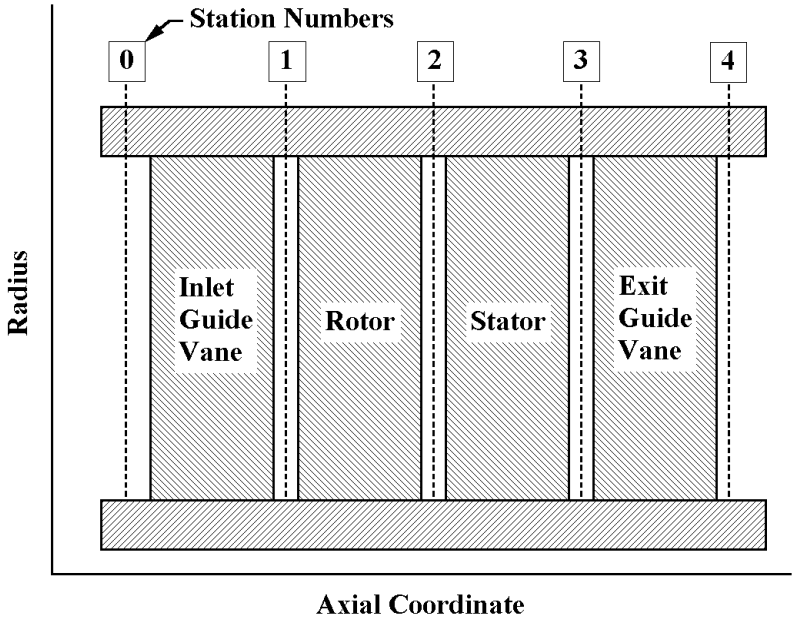

FIGURE 10-1 Stage Station Number Nomenclature

$$h_3 - h_1 = U(C_{\theta 2} - C_{\theta 1}) - (C_3^2 - C_1^2)/2 \tag{10-7}$$

Now consider a repeating stage design, i.e., a stage that is designed assuming it will be followed by another identical stage. This means that all velocity components at the stator exit and rotor inlet must be identical. Let us further require that $C_{z2} = C_{z1}$. Then Eqs. (10-3) through (10-7) yield

$$R = 1 - (C_{\theta 2} + C_{\theta 1})/(2U) \tag{10-8}$$

It follows that for a repeating stage design with $C_{z2} = C_{z1}$, all relevant stage velocity triangles can be specified in terms of the dimensionless performance parameters ϕ, ψ and R. For example, from Eqs. (3-1), (10-1), (10-2) and (10-8), it is easily shown that

$$C_{\theta 1}/U = C_{\theta 3}/U = 1 - R - \psi/2 \tag{10-9}$$

$$C_{\theta 2}/U = 1 - R + \psi/2 \tag{10-10}$$

$$W_{\theta 1}/U = C_{\theta 1}/U - 1 = -R - \psi/2 \tag{10-11}$$

$$W_{\theta 2}/U = C_{\theta 2}/U - 1 = \psi/2 - R \tag{10-12}$$

$$\tan\beta_1 = (1 - R - \psi/2)/\phi \tag{10-13}$$

$$\tan\beta_2 = (1 - R + \psi/2)/\phi \tag{10-14}$$

$$\tan\beta_1' = -(R + \psi/2)/\phi \tag{10-15}$$

$$\tan\beta_2' = (\psi/2 - R)/\phi \tag{10-16}$$

Specifications for the inlet and exit guide vanes have not been discussed yet. The simplest specification is to require C_z to be constant across these vanes and $C_{\theta 0} = C_{\theta 4} = 0$.

10.2 APPLICATION TO STAGE DESIGN

Development of the dimensionless performance parameters in the previous section assumed constant C_z (or ϕ) throughout the stage. But C_z is also governed by basic fluid dynamics, as has been described in Chapter 7. In particular, C_z must satisfy some form of the normal equilibrium equation. This means that the stage dimensionless performance can only be specified at one radius for any axial station. The radius at which the dimensionless performance is specified will be designated as r_c, and a subscript, c, will be used to identify all parameters on that radius. Hence, the stage dimensionless performance will be specified by

$$\phi_c = C_{zc}/U_c \tag{10-17}$$

$$\psi_c = (C_{\theta 2c} - C_{\theta 1c})/U_c \tag{10-18}$$

$$R_c = 1 - (C_{\theta 1c} + C_{\theta 2c})/(2U_c) \tag{10-19}$$

In Chapter 7, normal equilibrium and conservation of mass were combined to complete the solution. That requires that the stage design be specific to the working fluid and Mach number level for which it is to be applied. In this chapter, it is useful to avoid imposing those constraints in the interest of a more general investigation of design alternatives. This will also accommodate the general industrial repeating stage design application discussed earlier in this chapter. The application-specific design problem will be considered in chapter 11.

Hence the problem to be addressed in this chapter is illustrated in Fig.10-2. The hub, shroud and reference radii will all be held constant through the stage. The stage will be designed as a repeating stage with ϕ_c constant throughout the stage, i.e., C_{zc} is constant on the reference radius. The absence of an equation of state and Mach number dependence precludes a meaningful calculation of losses from the models presented in Chapter 6, so the flow will be considered to be isentropic. Common design practice is to require constant total enthalpy from hub to shroud, which will be assumed to be the case in stage design studies considered in this chapter. It will be shown later in this chapter that it is relatively easy to include provisions to relax many of these constraints in an actual computerized stage design system to obtain a more general design capability. But that does not add any benefits to developing an understanding of the merits of alternate dimensionless performance specifications. The flow profiles at other radii will be supplied by applying the simple, isentropic normal equilibrium

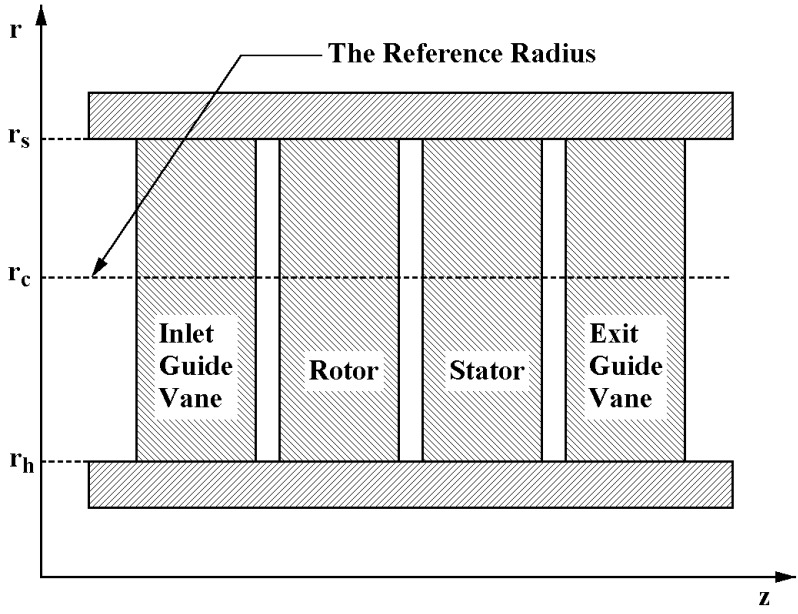

FIGURE 10-2 The Stage Design Application

equation to a prescribed tangential velocity distribution. A general vortex type equation is applied at the rotor inlet.

$$C_{\theta 1} / U_c = (1 - R_c)(r_c / r)^n - (\psi_c / 2)(r_c / r)^m \tag{10-20}$$

where the exponents n and m are specified. From Eq. (10-9), it can be seen that this vortex equation is consistent with the dimensionless performance specifications at $r = r_c$. It will be seen later in this chapter that this vortex equation includes a wide variety of design styles, including the styles most commonly used. At the rotor exit, the constant total enthalpy assumption is used.

$$C_{\theta 2} / U_c = C_{\theta 1} / U_c + \psi_c (r_c / r) \tag{10-21}$$

For our repeating stage design problem, the other tangential velocity distributions are given by

$$C_{\theta 3} / U_c = C_{\theta 1} / U_c \tag{10-22}$$

$$C_{\theta 0} / U_c = C_{\theta 4} / U_c = 0 \tag{10-23}$$

The basic normal equilibrium equation is obtained from Eq. (3-30) by expressing it in stationary coordinates, neglecting streamline curvature and entropy gradients.

For the present case, the meridional coordinate is z, and the normal coordinate is r. This yields

$$C_z \frac{\partial C_z}{\partial r} + \frac{C_\theta}{r} \frac{\partial r C_\theta}{\partial r} = \frac{\partial H}{\partial r} \tag{10-24}$$

In cases to be considered in this chapter, the total enthalpy gradient will also be zero, but this term has been retained to accommodate provision for a more generalized work distribution. Equation (10-24) can be integrated numerically, with the constant of integration supplied by the known value of ϕ_c. Hence, the dimensionless velocity components and velocity triangles can be computed at all of the axial stations on Fig. 10-1 and at all radii once values for ϕ_c, ψ_c, R_c, n and m are supplied. Specified values of the hub, shroud and reference radii are also required. The design of blades to produce these velocity triangles is discussed in the following section.

Practical application or evaluation of these ideal stage designs is provided through the performance analysis procedures described in Chapters 6 through 9. The ideal stage design is accomplished over a range of radii sufficient to pass the desired mass flow for the intended applications. The performance analysis then selects the portion of the blades designed that are actually required, using the annulus sizing capability described in Chapter 7, Section 7.7.

10.3 BLADE DESIGN

Once the velocity component and velocity triangle distributions have been computed at the entrance and exit stations for all blade rows to be designed, the blade geometry to be used can be computed. Some basic geometry data must be specified to carry out the blade design process. Several alternative specifications are possible, but this writer finds the following specifications to be effective and relatively easy to supply:

- Specify the blade camberline and profile type to be used.
- Specify the number of blades in the blade row, Z.
- Specify the chord, c, at the hub, reference and shroud radii.
- Specify the thickness-to-chord ratio, t_b / c, at the hub, reference and shroud radii.
- If required, specify the location of maximum camber, a / c.
- For double-circular-arc blades specify the leading and trailing edge nose radii, r_0. A convenient specification is the ratio, r_0 / t_b.
- Specify the difference between the incidence angle and the design incidence angle, $\Delta i = i - i^*$, at the hub, reference and shroud radii.

Values of c, t_b / c and Δi at other radii are obtained by interpolation from the three points supplied. The local solidity is given by

$$\sigma = cZ / (2\pi r) \tag{10-25}$$

The blade angle sign convention used in this book generally results in a negative turning angle for rotors and inlet guide vanes. To apply the blade geometry procedures of Chapter 4 and the empirical cascade performance models of Chapter 6 in these cases, it is necessary to change the signs on all flow and blade angles. After the blade design is complete, the signs of all angles are changed back to obtain blade geometry consistent with the sign convention used. The blade design process will be illustrated for the rotor blade, with the understanding that this sign adjustment is required. Design of other blade rows is handled in the same manner. The procedure is as follows:

1. Initialize the blade inlet and discharge angles equal to the relative flow angles, i.e., $\kappa_1 = \beta'_1$, $\kappa_2 = \beta'_2$.
2. Compute all other cascade geometry from κ_1 and κ_2 and the above geometry specifications, using the procedures of Chapter 4.
3. Compute i^* and δ^* using the procedures of Chapter 6.
4. Recompute the blade inlet and discharge angles from $\kappa_1 = \beta'_1 - i^* - \Delta i$ and $\kappa_2 = \beta'_2 - \delta^*$.
5. Repeat Steps 2 through 4 until convergence on κ_1 and κ_2 is achieved.

When the blades have been designed at all radii, all data required for the performance analysis are available. Detailed camberline and blade profile data can also be obtained as described in Chapter 4.

10.4 SELECTING THE STAGE PERFORMANCE PARAMETERS

It may appear that the designer has a vast array of choices for stage design through the basic performance specifications of ϕ_c, ψ_c, R_c, n and m. This is certainly true to some degree, but practical considerations dramatically reduce the designer's choices. When recommendations from the literature, gained from past stage design experience, are considered, the designer's range of choices actually become quite limited. Figures 10-3 through 10-5 illustrate practical constraints. Here, it is assumed that the relative velocity ratio across any blade row should not be less than 0.7. This is an adjusted de Haller stall limit obtained from Eq. (9-17) using the limit expressed in Eq. (9-18) and with $t_b / c = 0.1$. Noting that the minimum relative velocity ratio will almost always occur at either the hub or shroud radius, it is doubtful that designing for lower velocity ratios at the reference radius would be a wise choice. Eqs. (10-11) and (10-12) can be used to express the rotor blade relative velocity ratio as

$$\frac{W_2}{W_1} = \sqrt{\frac{\phi_c^2 + (\psi_c / 2 - R_c)^2}{\phi_c^2 + (\psi_c / 2 + R_c)^2}} \tag{10-26}$$

Similarly, for the stator, Eqs. (10-9) and (10-10) yield

$$\frac{C_3}{C_2} = \frac{C_1}{C_2} = \sqrt{\frac{\phi_c^2 + (1 - R_c - \psi_c / 2)^2}{\phi_c^2 + (1 - R_c + \psi_c / 2)^2}} \tag{10-27}$$

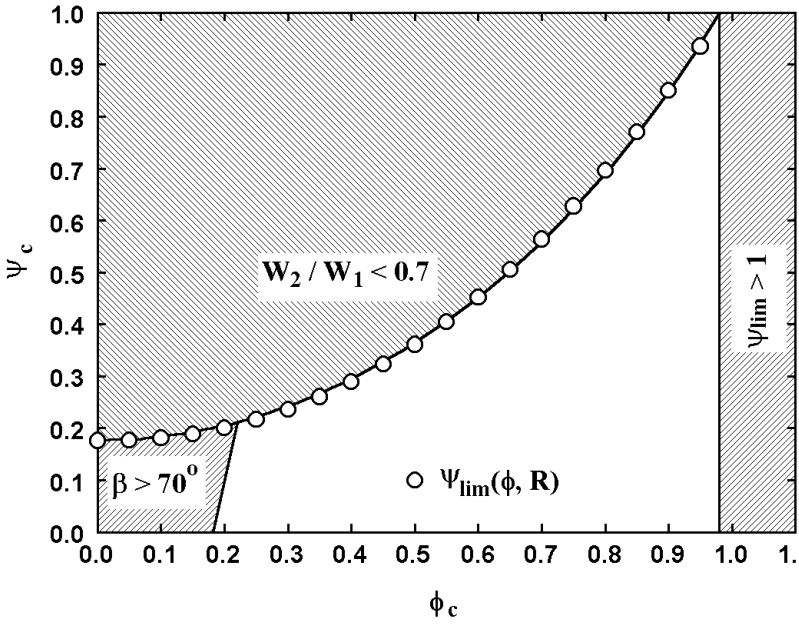

FIGURE 10-3 ψ-ϕ **Limits for 50% Reaction**

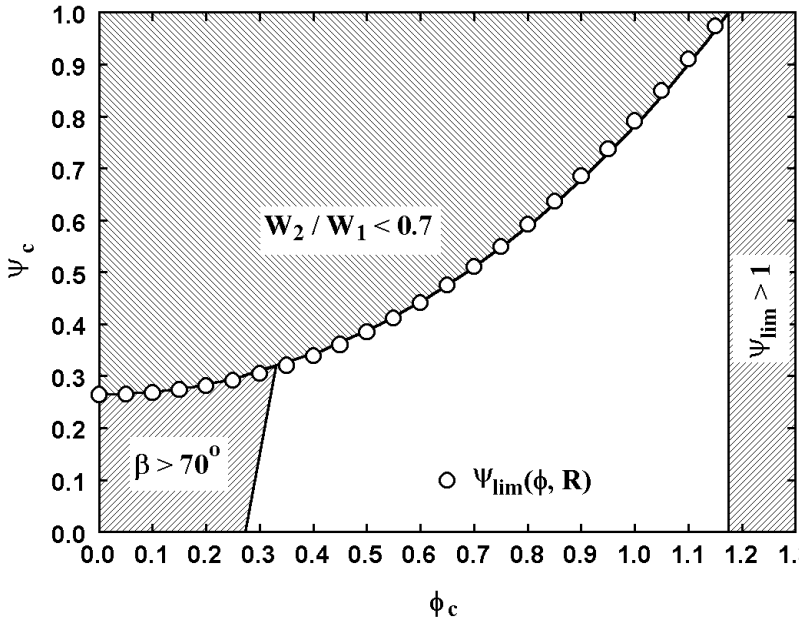

FIGURE 10-4 ϕ-ψ **Limits for 25% and 75% Reaction**

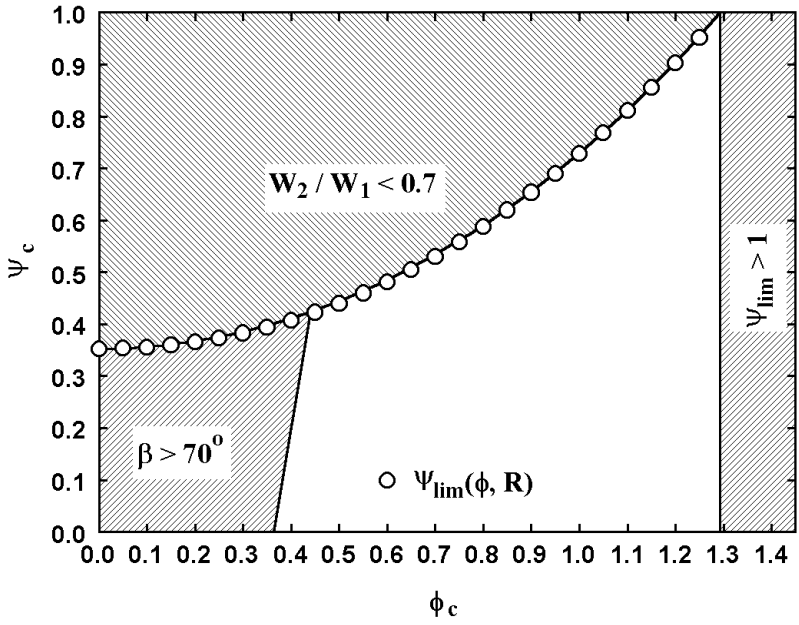

FIGURE 10-5 ϕ-ψ Limits for 0% and 100% Reaction

Eqs. (10-26) and (10-27) yield identical results for 50% reaction, i.e., the velocity triangles for the rotor and stator are identical (except for the sign convention). If these equations are applied for 25% and 75% reaction, it can also be seen that the minimum velocity ratio will be the same for both cases. The minimum simply appears on different blade rows for these two cases. Thus, the restrictions imposed by the velocity-ratio limit are symmetrical about $R_c = 0.5$. It can be useful to specify the work coefficient as some fraction of the value at this velocity-ratio limit to more easily choose practical values. This is easily done using the following empirical correlation for ψ_c corresponding to the velocity ratio of 0.7.

$$\psi_{\lim}(\phi, R) = \frac{6\hat{R}}{17} + 0.85\left(\frac{0.5}{\hat{R}}\right)^{1.18} \phi^{\left(2+0.1/\hat{R}\right)} \tag{10-28}$$

$$\hat{R} = 0.5 + |R - 0.5| \tag{10-29}$$

Results from this empirical equation are illustrated in Figs. (10-3) through (10-5).

Another constraint used on Figs. 10-3 through 10-5 is that the absolute values of all flow angles should not exceed 70°. Larger flow angles are likely to be impractical with respect to maintaining an acceptable throat area. Beyond that, many of the empirical cascade performance correlations of Chapter 6 are limited to flow

angles less than 70°, which is sufficient reason to impose this limit. Noting that $\beta_3 = \beta_1$, Eqs. (10-14) and (10-15) can be used to express this limit as approximately

$$\psi_c / 2 \le 2.75\phi_c - R_c \tag{10-30}$$

$$\psi_c / 2 \le 2.75\phi_c + R_c - 1 \tag{10-31}$$

Note that the restrictions imposed by this constraint are also symmetrical with respect to $R_c = 0.5$. Thus, these simple practical considerations have substantially reduced the range of choices for ϕ_c and ψ_c. It can also be noted that 50% reaction permits designing for the lowest values of ϕ_c and ψ_c. Indeed, as reaction increases or decreases from 50%, the major impact seen in Figs. 10-3 through 10-5 is that the acceptable range of design choices for ϕ_c moves toward higher values. There is also a reduction in the range of acceptable values of ψ_c for a given value of ϕ_c, but that effect is relatively minor.

Another important consideration is obtaining an acceptable surge margin, i.e., an acceptable flow range between the flow rate at the design point and the flow rate at which surge occurs. Alternatively, surge margin may be expressed in terms of the difference in discharge pressure between the design point and the surge point. It is clear that improved surge margin can be obtained by designing for a steeper slope on the constant speed pressure-flow characteristics. This resists the trend for increased losses or abrupt stalls to force the characteristic toward an unstable positive slope as the flow rate is reduced. Cumpsty (1989) notes that it is useful to approximate the work input curve in the form

$$\psi = 1 - \phi(\tan\beta_1 - \tan\beta_2') \tag{10-32}$$

This relation follows directly from Eqs. (10-13) and (10-16). The advantage of this form of the work input equation is that the flow angles involved are both discharge angles relative to the upstream blade row. It was shown in chapter 6 that the deviation angle is a very weak function of incidence angle. Hence, these flow angles can be considered to be approximately constant over a speed line. As illustrated in Fig. 10-6, this can be used to approximate Eq. (10-32) by

$$\psi \approx 1 - (1 - \psi_c)\phi / \phi_c \tag{10-33}$$

It follows that the surge margin will be improved by choosing lower values of both ϕ_c and ψ_c. From Eqs. (10-13), (10-16) and (10-32) it is easily shown that the slope of ψ as a function of ϕ will be positive if $\psi_c > 1$ is selected. This is certainly inconsistent with a reasonable surge margin. Hence, $\psi_{lim} > 1$ is treated as a third constraint on Figs. 10-3 through 10-5. Cumpsty (1989) also notes that the slope of the work-input characteristic is important to resist the influence of local total pressure distortions, even at operating conditions far from surge. He illustrates this by approximating the flow as incompressible, such that

$$P_t = P + \tfrac{1}{2}\rho W^2 = P + \rho U^2\phi^2 / \cos^2\beta' \tag{10-34}$$

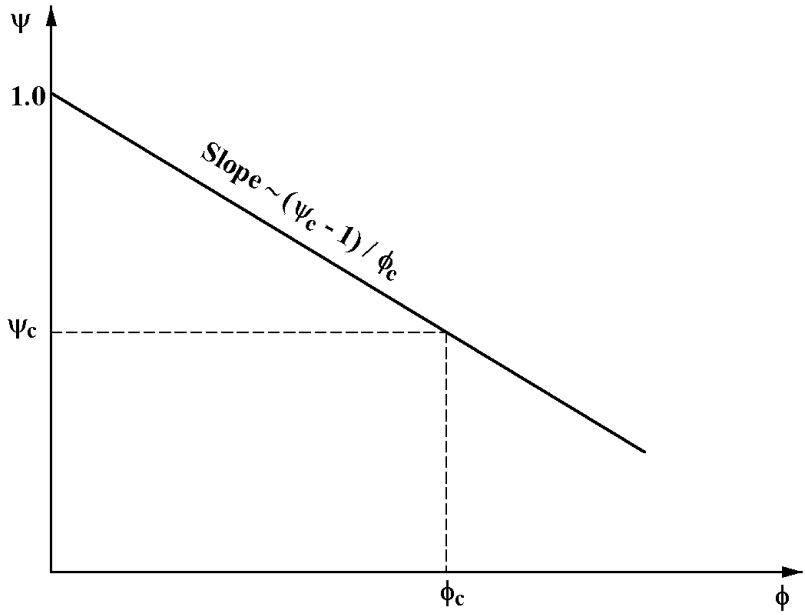

FIGURE 10-6 Approximate Work-Input Characteristic

Hence a local perturbation in total pressure, within an essentially constant static pressure flow field, can be approximated by

$$\delta P_t = 2\rho U^2 \phi \delta\phi / \cos^2 \beta' \tag{10-35}$$

It follows that a local deficit in total pressure will produce a local deficit in ϕ. If the work-input characteristic is sufficiently steep, the corresponding increase in ψ will reduce, and possibly eliminate, the total pressure deficit.

Smith (1958) provides a more detailed analysis of the capacity of a stage design to resist local total pressure deficits. In a discussion at the end of the paper by Smith, Ashley reports that the NACA had independently arrived at almost exactly the same result. Using arguments analogous to Eq. (10-35), Smith developed an equation to express the magnitude of a pressure deficit, $(\delta P_t)_{out}$, at the stage exit caused by an local inlet deficit, $(\delta P_t)_{in}$. He expressed this in terms of a parameter, R_R, which he called the recovery ratio.

$$R_R = 1 - \frac{(\delta P_t)_{out}}{(\delta P_t)_{in}} \tag{10-36}$$

It follows that for $R_R = 1$, the inlet total pressure deficit has been completely removed at the stage exit. For the case corresponding to the present dimensionless

performance parameters at the reference radius, Smith's recovery ratio can be expressed as

$$R_R = (\cos^2\beta_1 \tan\beta_1 - \cos^2\beta_2' \tan\beta_2')/\phi + \cos^2\beta_1 \cos^2\beta_2' \tan\beta_1 \tan\beta_2')/\phi^2 \quad (10\text{-}37)$$

Once again, it can be shown that R_R is symmetrical about R = 0.5. Figs. 10-7 through 10-9 show typical results for various values of reaction. To maintain reasonable values of ψ_c in these predictions, ϕ_c was constrained to the limits shown in Figs. (10-3) through (10-5), and Eq. (10-28) was used in the form

$$\psi_c = K_c \psi_{\lim}(\phi_c, R_c) \quad (10\text{-}38)$$

While values of R_R = 1 are certainly not required, it is expected that small or negative values should be avoided where possible. Based on results similar to those shown in Figs. 10-7 through 10-9, Smith suggested that values of $\phi_c < 0.5$ are preferred. Indeed, $\phi < 0.5$ at all radii would be preferred, which is a much stronger constraint. Clearly, if ϕ_c = 0.5 were imposed as an upper limit on Figs. 10-3 through 10-5, the range of choices available to the designer would be narrow. This is not considered to be appropriate in light of the many successful axial-flow compressor designs that have used significantly higher values of ϕ_c. But there does appear to be a definite trend toward lower values of ϕ_c in more modern

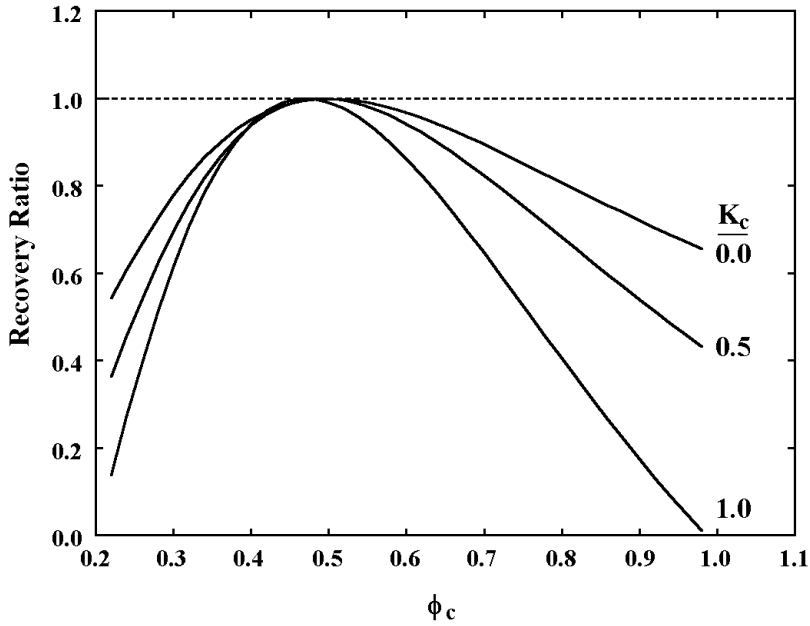

FIGURE 10-7 R_R for 50% Reaction

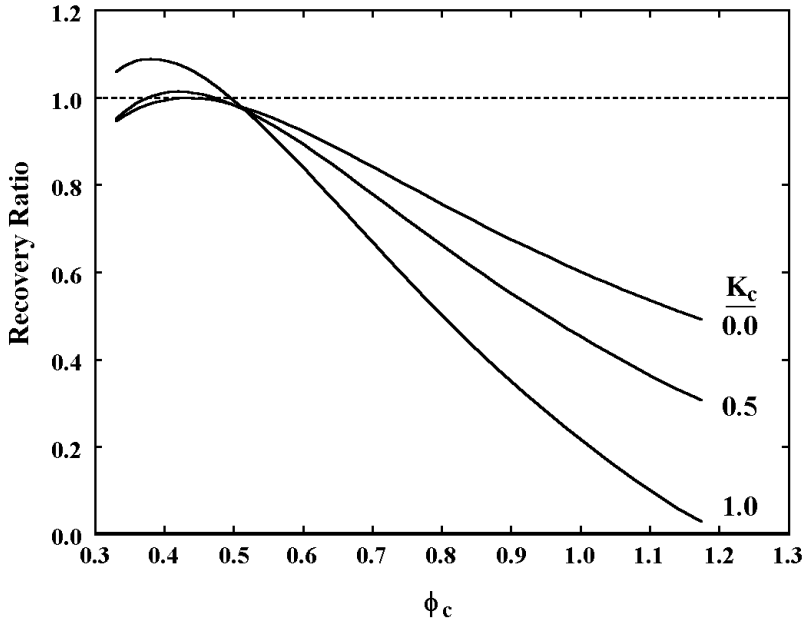

FIGURE 10-8 R_R **for 25% and 75% Reaction**

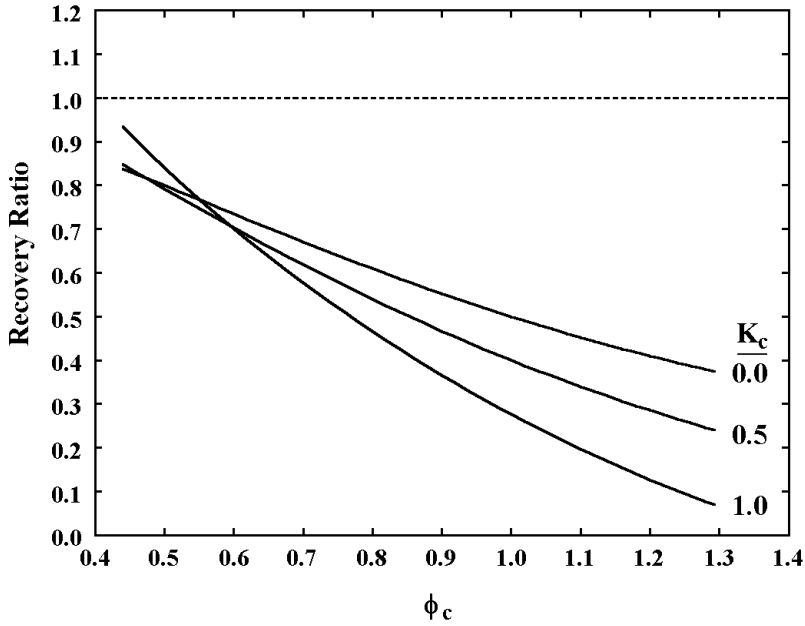

FIGURE 10-9 R_R **for 0% and 100% Reaction**

designs. Smith also concluded that the recovery ratio is not a strong function of reaction, which may be somewhat questionable. It is evident that $R_R < 1$ is to be expected for any practical combination of ϕ_c and ψ_c when R_c is 0 or 1.

Other guidance available in selection of ϕ_c, ψ_c and R_c are more in the form of opinions and rule-of-thumb practices. It has been common practice to favor 50% reaction designs, based on the intuitive benefit expected from distributing the flow diffusion load equally between the rotor and stator. Sometimes slightly higher reaction is recommended based on the assumption that rotors are slightly more efficient than stators. Similarly, designers seem to be most comfortable with choosing $\psi_c \leq 0.4$ in most cases. None of these opinions have been well substantiated by either experiment or analysis. Indeed, such guidelines are probably rather academic, since the selection of ϕ_c, ψ_c and R_c is dependent on many other factors. The swirl vortex type discussed in the next section of this chapter is very important. That determines the stage performance at other radii, and may have a significant influence on the choice of the reference radius performance parameters. Also, the developments in this chapter do not consider the effect of the Mach number level, which can have important consequences and impose definite constraints. That can be illustrated by a design goal common to nearly all axial-flow compressor designs, i.e., achieving the maximum mass flow per unit frontal area and the minimum number of stages. For aircraft engine compressors this permits essential size and weight reductions, while for industrial compressors the important benefit is reduced size and cost. In either case, this immediately encourages selection of larger values of ψ_c and ϕ_c, although lower values of ϕ_c are generally preferred. This might be resolved by simply designing for a higher speed to satisfy both needs. But Mach number effects impose definite limits on that approach as well as result in performance penalties when the approach is used.

10.5 SELECTING THE SWIRL VORTEX TYPE

In addition to the reference radius performance parameters, it is necessary to select the vortex type by specifying n and m in Eq. (10-20) to set the rotor inlet C_θ distribution. The C_θ distributions at other stations are given by Eqs. (10-21) through (10-23) for a constant-work, repeating stage. When the C_θ distributions are known, the C_z distributions at all stations are obtained by solving Eq. (10-24). Then the velocity triangles are known at all radii for all stations. If those velocity triangles are acceptable, the blades can be designed as described in Section 10.3. At this point in the design process, fluid dynamic data are available at all radii and must be evaluated. The same design preferences and practical limits considered relative to the reference radius certainly are relevant at other radii as well. It will be seen that problems associated with excessive flow diffusion or expected Mach number limits almost always occur first on the end-walls, usually at the rotor shroud and stator hub locations. It is not uncommon for an apparently very conservative selection of ϕ_c, ψ_c and R_c to produce unacceptable performance parameters at other radii. In the following sections, some commonly used vortex types will be reviewed to illustrate some of the important considerations in selecting the vortex type. To allow comparison of the various vortex types, a common design problem will be considered. All examples will be constant-work,

repeating stage designs. A hub-to-tip ratio of $r_h / r_s = 0.5$ will be considered, which is typical of the front stages in an axial-flow compressor. The reference radius will be set to $r_c / r_s = 0.8$, which approximately divides the annulus into two equal area passages. In principle, the reference radius is an arbitrary design parameter, but, in practice use of a typical mean-radius is usually necessary. Since C_z is constant on r_c, use of a mean-radius ensures approximate conservation of mass, which will be required when the stage is applied in a compressor. If the stage design deviates too far from this, the velocity triangles produced after sizing of the compressor annulus area may be very different from those intended.

10.6 FREE VORTEX FLOW

It is instructive to start with the popular free vortex design style, which is given by setting $n = m = 1$. From Eqs. (10-20) through (10-23) it can be shown that this yields constant angular momentum (rC_θ) profiles at all stations. If rC_θ and H are constant, Eq. (10-24) also yields constant C_z profiles. Indeed, since C_z is constant on the reference radius, this means that C_z is constant everywhere. Let us design a free vortex stage using very conservative dimensionless performance parameters. Following Smith, (1958) set $\phi_c = 0.5$. To provide significant margin from the loading limit, set $K_c = 0.8$. Choose $R_c = 0.5$ to distribute the loading equally between the rotor and stator. It would be expected that such conservative design specifications and such a simple type of vortex would certainly result in an acceptable design. Figures 10-10 and 10-11 show some of the important results obtained with these design specifications. It is apparent from the flow angle distributions that this design will require a highly twisted rotor blade, which may pose structural and manufacturing problems. The stator blade will be highly staggered to match flow angles close to the 70° limit suggested earlier in this chapter. But more serious is the fact that the design yields a substantial region of negative reaction near the hub. This results in significant flow acceleration across the rotor, followed by significant deceleration across the stator. The stator is overloaded near the hub, and probably will stall. Since $\psi_h > 1$, stability is a concern, as discussed in Section 10.4. The unacceptable features of this example could have been anticipated. Since ϕ is constant across the blade rows at all radii, Eq. (10-8) can be applied at any radius to predict the reaction. From Eq. (10-20), free vortex flow yields

$$C_{\theta 1} / U = (1 - R_c - \psi_c / 2)(r_c / r)^2 \tag{10-39}$$

Equation (10-21) requires

$$C_{\theta 2} / U = C_{\theta 1} / U + \psi_c (r_c / r)^2 \tag{10-40}$$

Substituting Eqs. (10-39) and (10-40) into Eq. (10-8) yields

$$R = 1 + (R_c - 1)(r_c / r)^2 \tag{10-41}$$

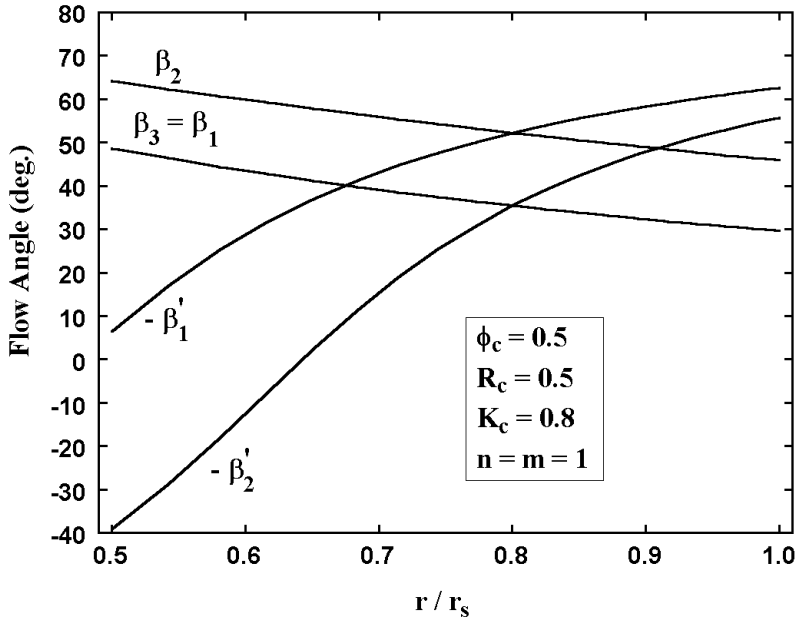

FIGURE 10-10 Flow Angle Distributions

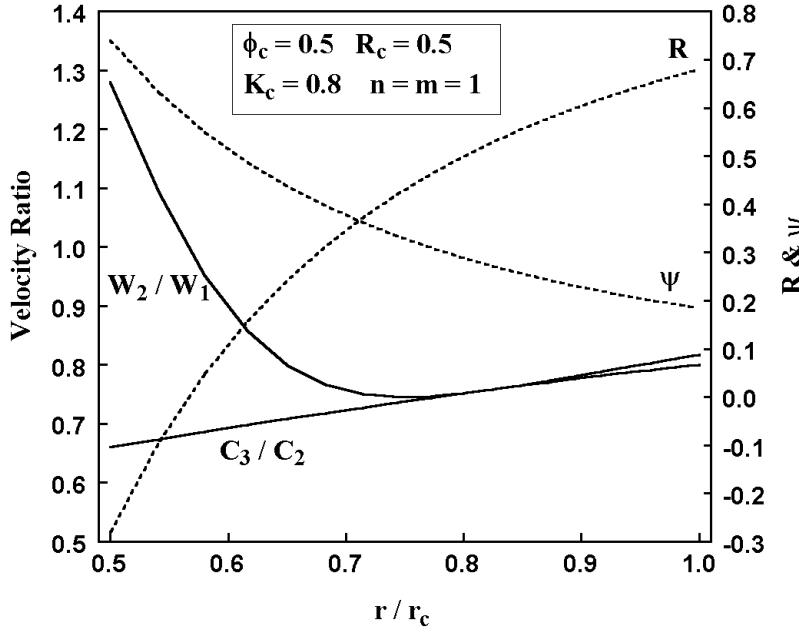

FIGURE 10-11 Blade Loading Distributions

Hence the condition to avoid negative reaction at the hub for free vortex flow is

$$R_c \geq 1-(r_h / r_c)^2 \tag{10-42}$$

For this example this requires $R_c \geq 0.609$. $R_c = 0.5$ can be maintained by requiring $r_h / r_c \geq 0.7071$. Since C_z is constant everywhere, the choice of r_c is quite arbitrary for free vortex flow. It is likely that R_h significantly greater than zero would be preferred, which can be easily obtained using Eq. (10-41). This simple example illustrates that selection of the dimensionless stage performance parameters is strongly influenced by the vortex type to be used and the radius-ratio range required.

Instead of refining the previous example, it is more useful to continue the discussion of free vortex flow with a more commonly used form obtained by adding the requirement that $C_{\theta 1} = C_{\theta 3} = 0$. The advantage of this form is that no inlet or exit guide vanes are required. From Eq. (10-9) this requires

$$\psi_c = 2(1-R_c) \tag{10-43}$$

To maintain a negative slope on the work-input characteristic, $\psi_c < 1$ is required. That requires $R_c > 0.5$, which means that the rotor is more highly loaded than the stator. To maintain a reasonable loading level in the rotor, it is desirable to specify the velocity ratio, $W_{2c} / W_{1c,}$ as well. Equations (10-26) and (10-43) yield

$$\phi_c^2 = \frac{(W_{2c} / W_{1c})^2 - (1-2R_c)^2}{1-(W_{2c} / W_{1c})^2} \tag{10-44}$$

Figure 10-12 is a (R_c, ϕ_c) design chart with W_{2c} / W_{1c} as a parameter, with the usual practical limits imposed. Clearly, Smith's recommendation of $\phi_c \leq 0.5$ requires rather high reaction. From Eq. (10-43) that also requires very low values of ψ_c. Thus, it may be difficult to follow Smith's recommendation while maintaining a reasonable stage work input coefficient. For example, Fig. 10-12 includes the (R_c, ϕ_c) mean-radius design point for the first stage of the NACA 5-stage axial-flow compressor (Sandercock et al., 1954). This is an actual example of a free vortex design with $C_{\theta 1} = 0$, which illustrates the type of compromise that may be required in a practical stage design.

To illustrate features of the free-vortex design, the basic specifications for the first stage of the NACA 5-stage axial-flow compressor were used to generate a stage design using the procedures presented in this chapter. Figure 10-13 shows the relevant flow angles for this design. A variable camber, highly twisted rotor blade will be required, although not as extreme as the earlier example. Figure 10-14 shows that the rotor tip inlet relative velocity is by far the largest velocity in the stage and will be the value to be evaluated in terms of Mach number levels. No general conclusion can be reached without specifying the stage inlet conditions and rotation speed, but the rotor tip will be the critical location. Indeed, as observed in chapter 9, the first stage of the NACA 5-stage compressor is a transonic design. The stator inlet and exit velocity levels are quite modest by comparison, so Mach number level should not be a concern. Figure 10-15 shows that the velocity ratios across the

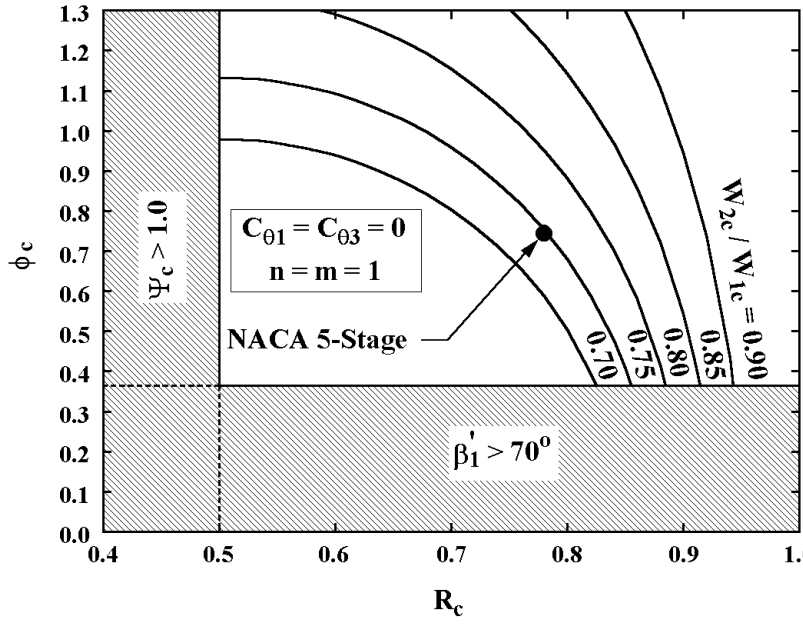

FIGURE 10-12 Free Vortex Design Chart

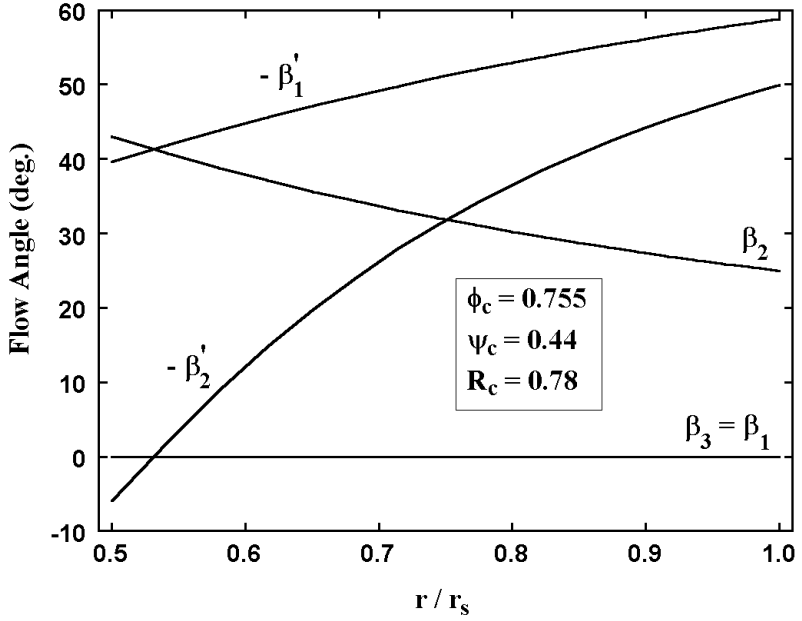

FIGURE 10-13 Free Vortex Flow Angles

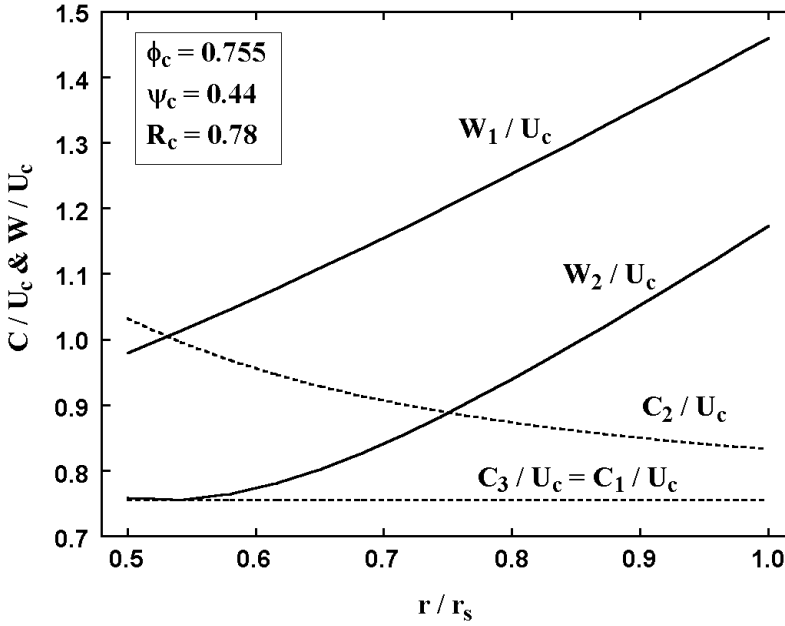

FIGURE 10-14 Free Vortex Velocities

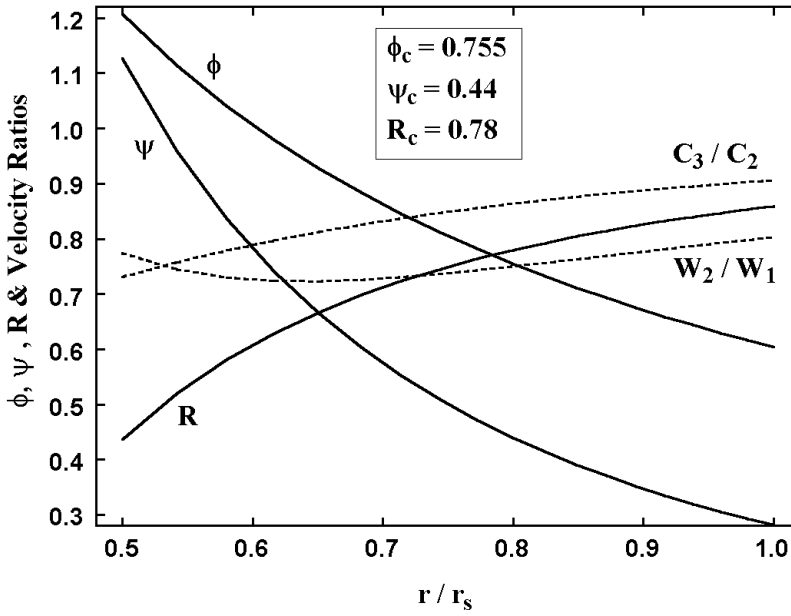

FIGURE 10-15 Free Vortex Performance Parameters

blades are relatively close to the de Haller limit on both the rotor and the stator. As seen in Figure 10-12, the design specifications correspond to a rotor relative velocity ratio at the reference radius of only 0.75, so this is really to be expected. The reaction is significantly positive at the hub, which has avoided the velocity ratio problems seen in Fig. 10-11 for the simple example considered earlier. A smaller value of ψ_c probably should be used to avoid the $\psi_h > 1$ condition and to improve the velocity ratios across the blade rows.

The blade design procedures described earlier in this chapter were used to design double-circular-arc blades to match the velocity triangles. The blades were designed with constant chord, and with $t_b / c = 0.1$. The number of blades in each row was set to yield $\sigma = 1$ at the reference radius. Figure 10-16 shows the camber and stagger angle distributions for the rotor and the stator. As expected, a highly twisted, variable camber rotor blade is required. Variations of camber and stagger angles with radius on the stator are relatively modest. However, the radial variation in $\beta_{2,}$ as seen in Fig. 10-13, is probably too great to seriously consider using a constant camber, constant stagger stator blade for this stage.

10.7 CONSTANT REACTION VORTEX FLOW

Another vortex type occasionally suggested is obtained by setting $n = -1$ and $m = 1$. Inserting these values into Eqs. (10-20) and (10-21) and substituting

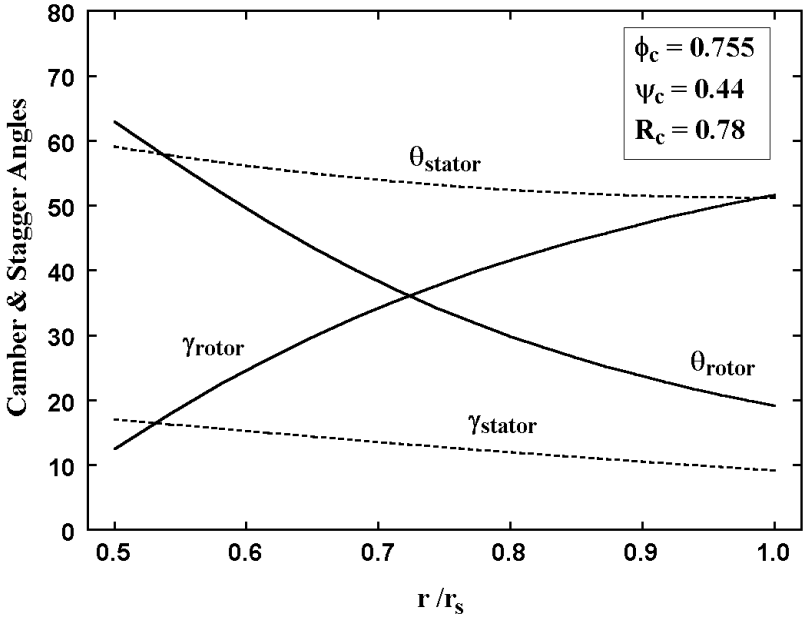

FIGURE 10-16 Free-Vortex Blade Design

into Eq. (10-8) appears to yield a constant reaction design, which is the title commonly applied to this vortex type. It must be recognized that, normally, constant reaction will not be achieved, since ϕ is not generally constant across the rotor as is assumed by Eq. (10-8). This is easily illustrated by repeating the "conservative" design used as an example of free vortex flow in the previous section. Figures (10-17) and (10-18) show results from that design with the constant reaction type of vortex. It is seen that the design is by no means that of constant reaction. Indeed, reaction is close to zero at the hub radius. Velocity ratios across both the rotor and stator are well below the de Haller limit, which is not very encouraging for operation at the stage's design point. But the major problem is that the axial velocity at the rotor discharge drops to zero below the tip radius. The stage design software used restricts the axial velocity from becoming negative to prevent fatal errors in the analysis. So the zone of zero axial velocity is actually a reverse flow zone. Data predicted in this zone are not accurate, as indicated by the dashed lines near the shroud radius. Once again, it is seen that the specific vortex style can produce an unacceptable design, even though the dimensionless performance parameters appear to be rather conservative. It is quite evident that the large variation in axial velocity between the rotor exit and inlet stations has completely nullified the intention of achieving an essentially constant reaction.

One of the exercises at the end of this chapter will be to show that the radial gradient of reaction for any constant work, repeating stage is given by

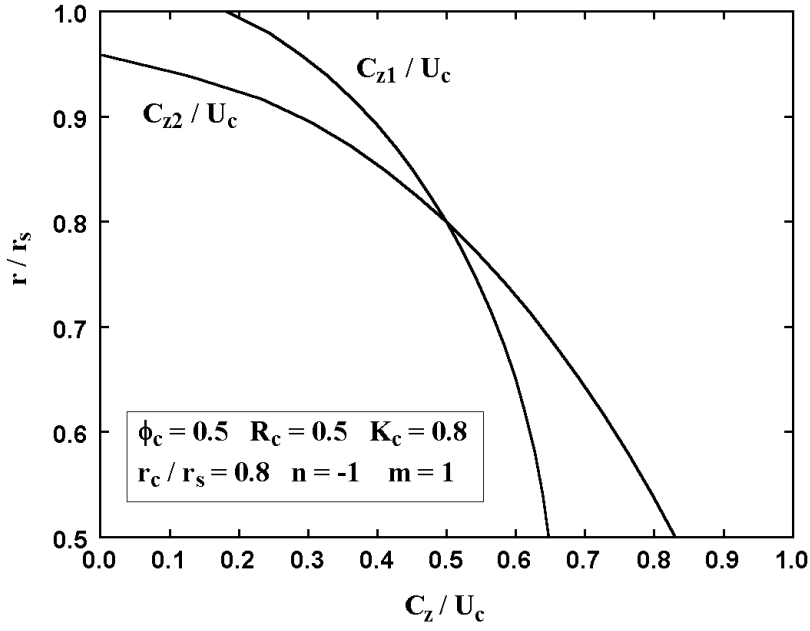

FIGURE 10-17 Axial Velocity Distributions

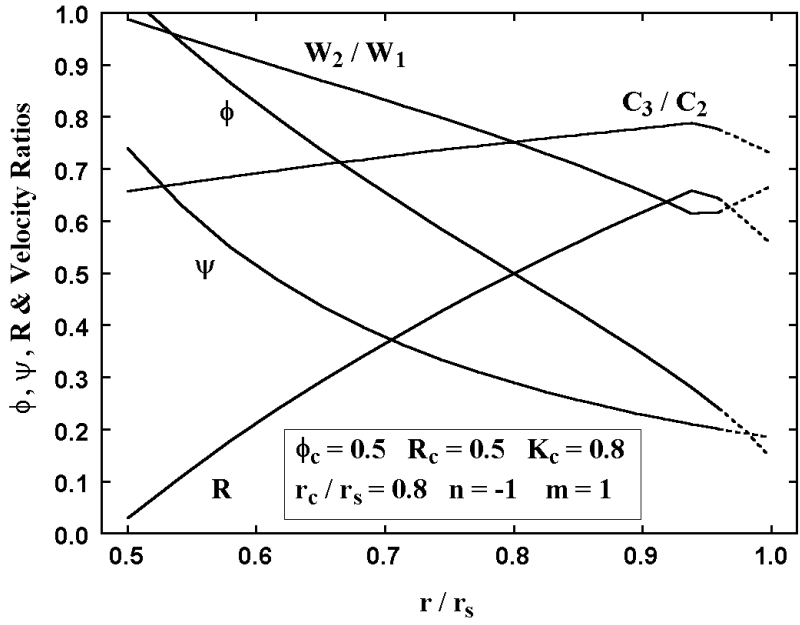

FIGURE 10-18 Performance Parameter Distributions

$$r_c \frac{\partial R}{\partial r} = 2(1-R_c)(r_c/r)^{(2+n)} + \psi_c[(r_c/r)^3 - (r_c/r)^{(2+m)}] \tag{10-45}$$

With n = -1 and m = 1, this yields

$$r_c \frac{\partial R}{\partial r} = 2(1-R_c) r_c / r \tag{10-46}$$

Equation (10-45) can be integrated to yield

$$R = R_c + 2(1-R_c)\ln(r/r_c) \tag{10-47}$$

Clearly, the only case for which this vortex type will yield constant reaction is when R_c = 1. For other values of R_c, Eq. (10-47) can be used to compute a value of R_c that will yield a desired value of reaction at the hub. It is clear that reaction is completely independent of ϕ_c and ψ_c. However, it will be possible to eliminate the reverse flow zone by increasing ϕ_c. Indeed, another exercise at the end of this chapter will be to show that the condition to avoid reverse flow at the rotor exit for any radius, r, for the constant reaction vortex style is

$$\phi_c^2 \geq 2(1-R_c)^2[(r/r_c)^2 - 1] + 2(1-R_c)\psi_c \ln(r/r_c) \tag{10-48}$$

Reverse flow will first occur at the rotor exit on the shroud. Hence Eq. (10-48) can be used to compute the minimum acceptable value of ϕ_c for any value of R_c using $r = r_s$. Alternatively, the value of R_c required to avoid reverse flow for any ϕ_c can be estimated from Eq. (10-48) by trial and error. In this way, it can be shown that values of ϕ_c down to 0.5 will be achievable for this case with no reverse flow if $R_c \geq 0.6$ is used. This limit was used to investigate the influence of ϕ_c and R_c on the stage design for this vortex type. The influence of ϕ_c is shown in Fig. 10-19. It is seen that ϕ_c has little influence on the velocity ratios across the blades. Increasing ϕ_c increases the inlet velocity for both blade rows. Since the loss is proportional to the inlet kinetic energy, this is expected to increase the losses. It may also lead to other problems due to the increased Mach number levels. The only real benefit from larger values of ϕ_c is the higher values of ψ_c obtained for the same value of K_c. The influence of R_c is shown in Fig. 10-20. Increasing R_c will increase the rotor inlet kinetic energy, raising concerns about loss and Mach number levels that are similar to the concerns regarding Fig. 10-19. The reduction of the stator inlet kinetic energy is some compensation for these concerns. The work coefficient is nearly independent of R_c for a specified K_c. Hub reaction and the minimum velocity ratio across the stator both benefit significantly from increased values of R_c. The minimum velocity ratio across the rotor appears a little erratic, which is caused by the location of the minimum value switching from the hub radius to the shroud radius. Probably the most notable observation is that there is an optimum value of R_c at about 0.79 that yields the highest minimum velocity ratio across

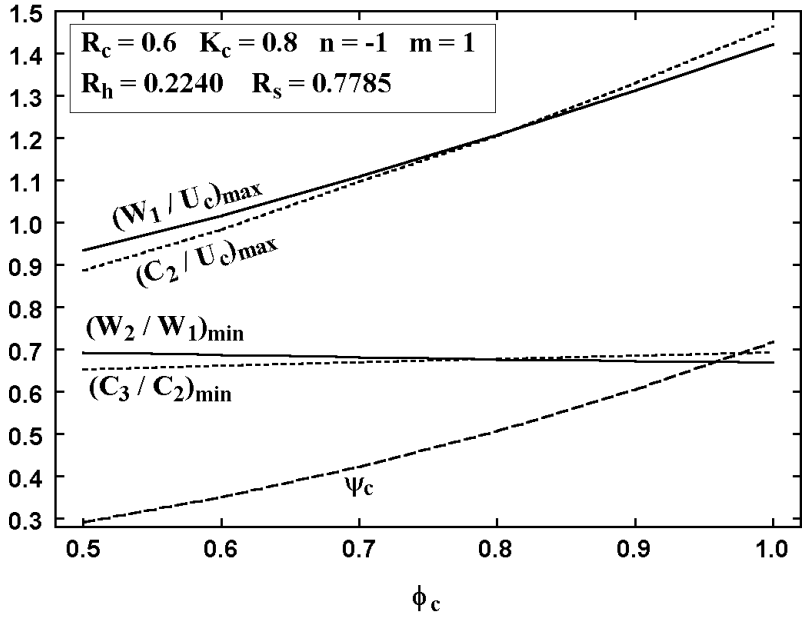

FIGURE 10-19 Influence of Flow Coefficient

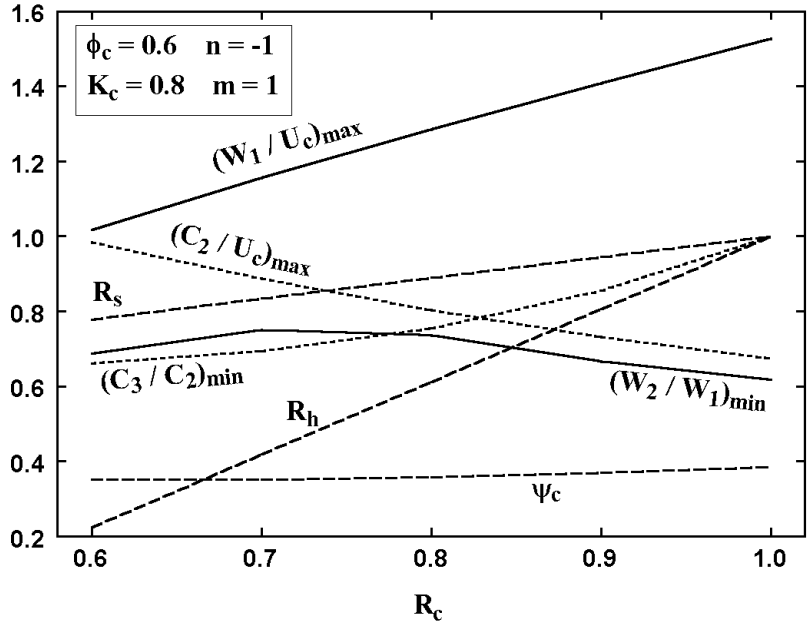

FIGURE 10-20 Influence of Reaction

either blade row. This would be expected to provide the best stall margin, assuming the increased rotor inlet Mach number level does not become the limiting factor. To investigate this more closely, a constant reaction vortex stage was designed based on this optimum. For the purpose of comparison, a free vortex stage was designed for the same set of dimensionless performance parameters. Figures 10-21 through 10-23 compare some of the more significant results. It is seen that the constant reaction vortex flow yields the lowest peak rotor inlet velocity and offers greater margin from stall as indicated by the velocity ratios across the blade rows. Both vortex types require a twisted, variable-camber rotor blade, but the variations are less extreme for the constant reaction vortex style. Twisted, variable-camber stator blades are required for both vortex types, with slightly more extreme variations for the constant reaction type of vortex. The work input coefficient distributions for both vortex types are identical, with $\psi_h = 0.913$, so the work input characteristics at all radii should have the desired negative slope. It can be concluded that the constant reaction vortex style does offer some advantages over the free vortex style for this specific set of dimensionless performance parameters, particularly with regard to increased stall margin.

The most important conclusion with regard to the constant reaction vortex style is that the usual claim that it yields blades of nearly constant reaction is simply not correct, unless R_c values that are very close to 1.0 are used. In other cases, it is necessary to choose a reaction at the reference radius that will yield an acceptable reaction at the hub, much like the case of the free vortex style. This is

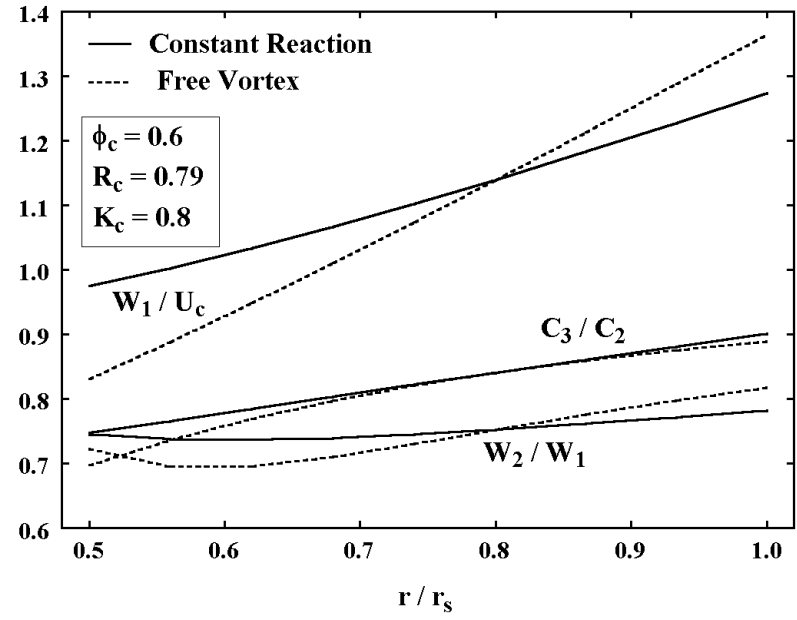

FIGURE 10-21 Comparison of Velocity Ratios

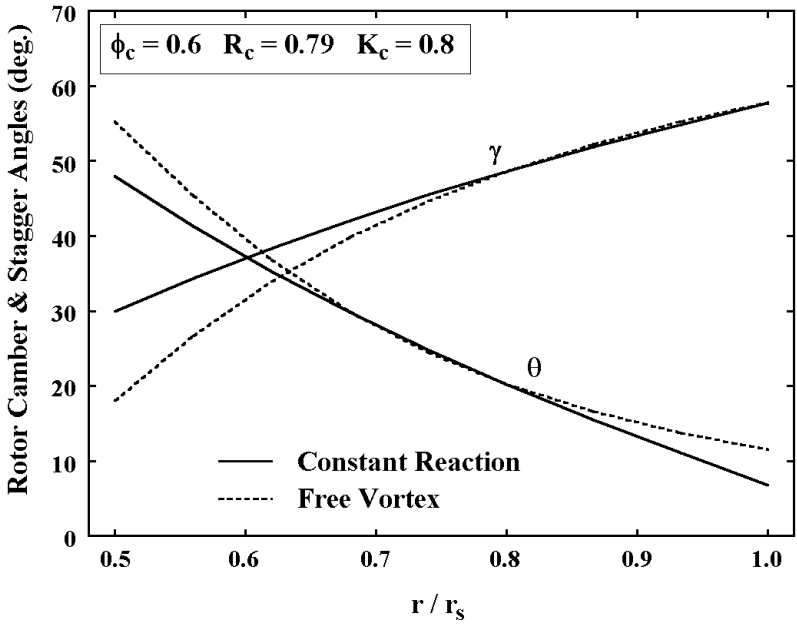

FIGURE 10-22 Comparison of Rotor Blade Geometry

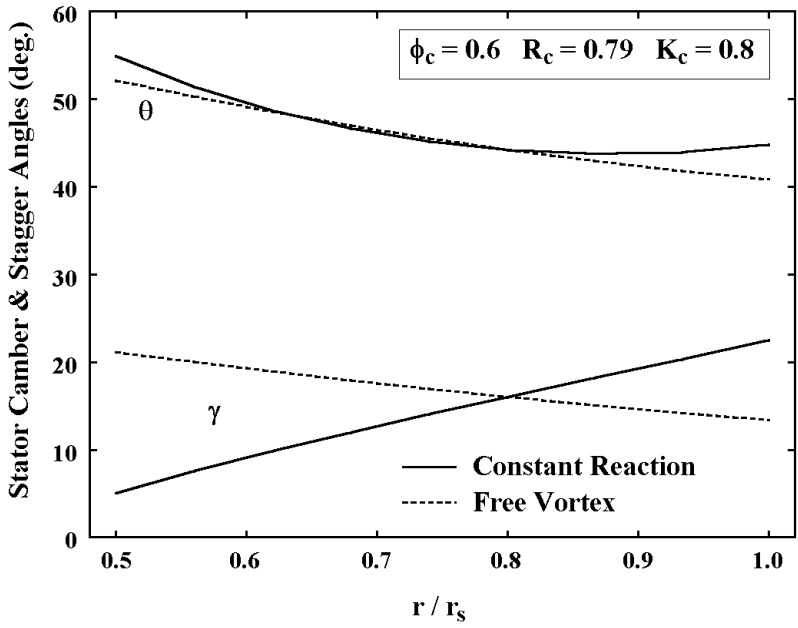

FIGURE 10-23 Comparison of Stator Blade Geometry

easily accomplished with the aid of Eq. (10-47), so effective use of the constant reaction vortex style is not too difficult. It is worth considering whether this vortex style can be modified so that it will more closely approximate a constant reaction stage. From Eq. (10-45) it is clear that there is really no alternate selections for m and n that will yield constant reaction. One of the exercises at the end of the chapter will be to show that the only possible constant reaction design is the 100% reaction case. A very modest reduction in the radial gradient of the reaction can be achieved by choosing n = -2 and m = 1, which yields

$$r_c \frac{\partial R}{\partial r} = 2(1 - R_c) \tag{10-49}$$

$$R = R_c + 2(1 - R_c)(r / r_c - 1) \tag{10-50}$$

This has the undesirable effect of producing steeper gradients near the shroud radius, to impose additional restrictions to avoid reverse flow. It is possible to more closely approximate constant reaction by choosing n = -1 or -2 and selecting $m > 1$. From Eq. (10-45) it can be seen that this introduces a negative contribution to the radial-gradient of R when $r < r_c$ to partially balance the usual positive gradient. However, it has the reverse and unfavorable effect when $r > r_c$. This approach is generally not too effective, but it could be considered for very specific applications.

10.8 CONSTANT SWIRL AND EXPONENTIAL VORTEX FLOWS

Horlock (1958) suggests that the exponential vortex style is often a good choice, and is obtained by setting $n = 0$ and $m = -1$. A very similar alternative is obtained by setting $n = m = 0$, which will be called the constant swirl vortex style. As seen from Eq. (10-20), the constant swirl vortex style yields constant $C_{\theta 1}$. With appropriate choices for ϕ_c, ψ_c, and R_c, these two vortex types may yield a constant-camber stator blade, possibly with a constant stagger angle as well. This is certainly attractive for reducing manufacturing cost and may offer other advantages, such as improved structural characteristics. From Eq. (10-45) it is easily shown that the reaction at any radius for exponential vortex flow is given by

$$R = R_c - 2(1 - R_c)(r_c / r - 1) \tag{10-51}$$

whereas for constant swirl vortex flow,

$$R = R_c - [2(1 - R_c) + \psi_c(r_c / r - 1) / 2](r_c / r - 1) \tag{10-52}$$

Hence the exponential vortex style has the advantage that the value of R_c required to achieve any desired hub reaction is easily determined. It is also clear that the exponential vortex flow will yield the higher hub reaction for any value of R_c. While these advantages tend to favor the exponential vortex style, the constant swirl vortex flow also has a definite advantage, as illustrated by Figs. 10-24 and 10-25. These figures show the difference in the stator camber angle and stagger angle between the hub and the shroud for stages designed with these two types of vortex. If the difference in camber angle is small enough, a constant camber stator blade can probably be used. Similarly, if the difference in stagger angle is small enough, a constant stagger stator blade can probably be used. It is clear that both vortex styles can yield a constant-camber stator blade if an appropriate value of R_c is chosen. It can be seen that the precise value of R_c required varies with ϕ_c. Indeed, it will also depend on K_c to some degree. Clearly, the prospects for achieving a stator blade with both constant camber and constant stagger angles are substantially better if the constant swirl vortex flow is employed.

To illustrate the advantages of constant swirl vortex flow, a stage was designed specifically to achieve a constant-camber, constant-stagger stator blade. The important stage performance data for this design are shown in Fig. 10-26. It will be noticed that this design used a lower value of K_c than has been used in previous examples. This was necessary to maintain a reasonable velocity ratio across the stator at the hub, which is typically the weakest area of a constant swirl or exponential vortex design. The reduced work input capability is not as pronounced as it may first appear. Indeed, Fig. 10-21 shows that, for similar reasons, a similar reduction in K_c would have been beneficial for the free vortex design as well. In comparison to the free vortex and constant reaction vortex designs in Fig. 10-21, it is seen that lower values of rotor-inlet relative velocity have been achieved. The basic limitations for this vortex style are associated with low values of R and C_3 / C_2 near the hub. Figure 10-27 shows the rotor and stator camber

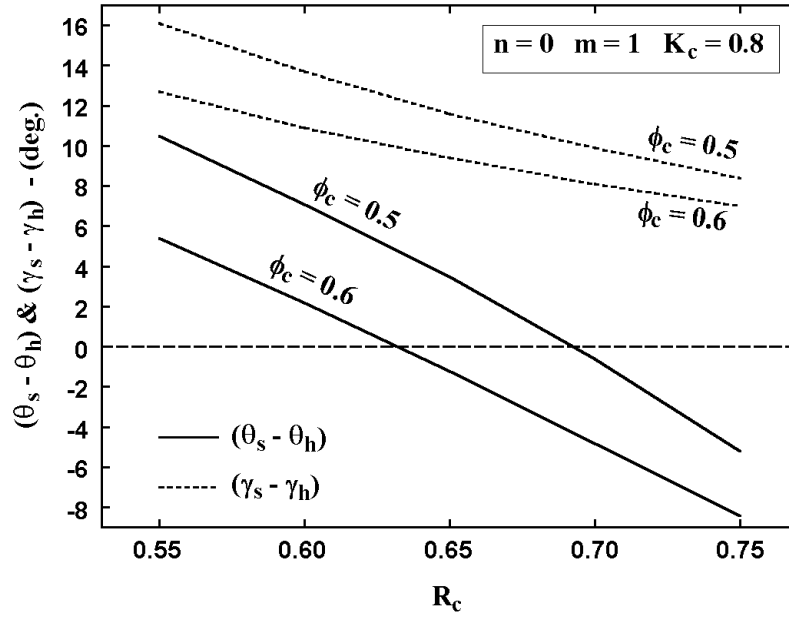

FIGURE 10-24 Exponential Vortex Stators

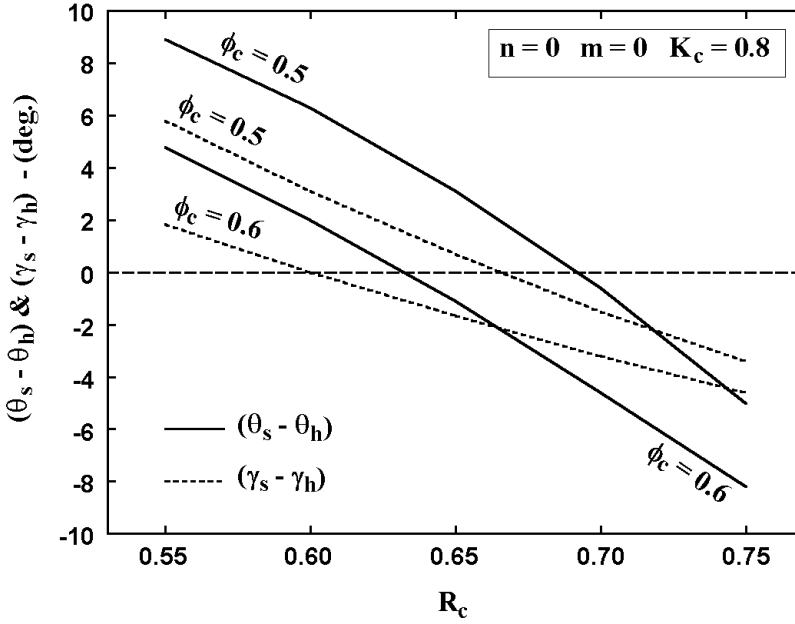

FIGURE 10-25 Constant Swirl Vortex Stators

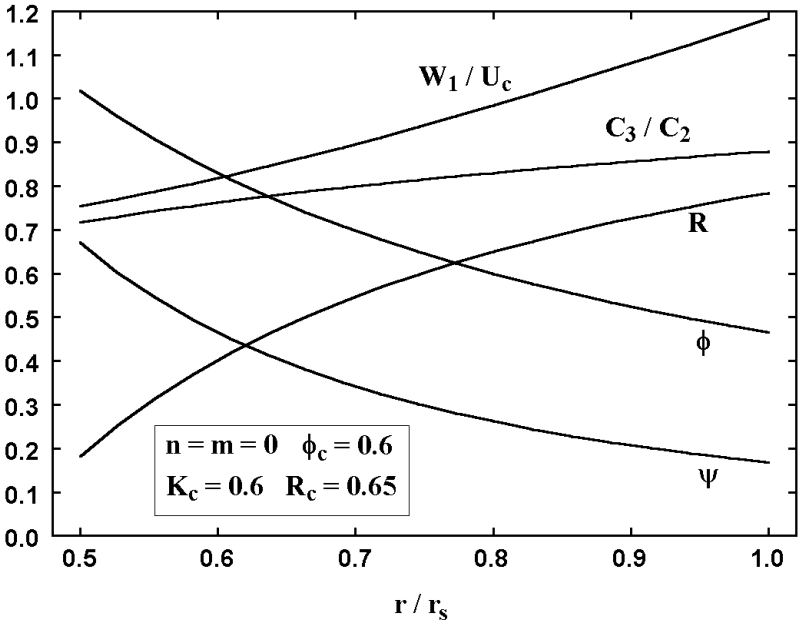

FIGURE 10-26 Constant Swirl Vortex Design Data

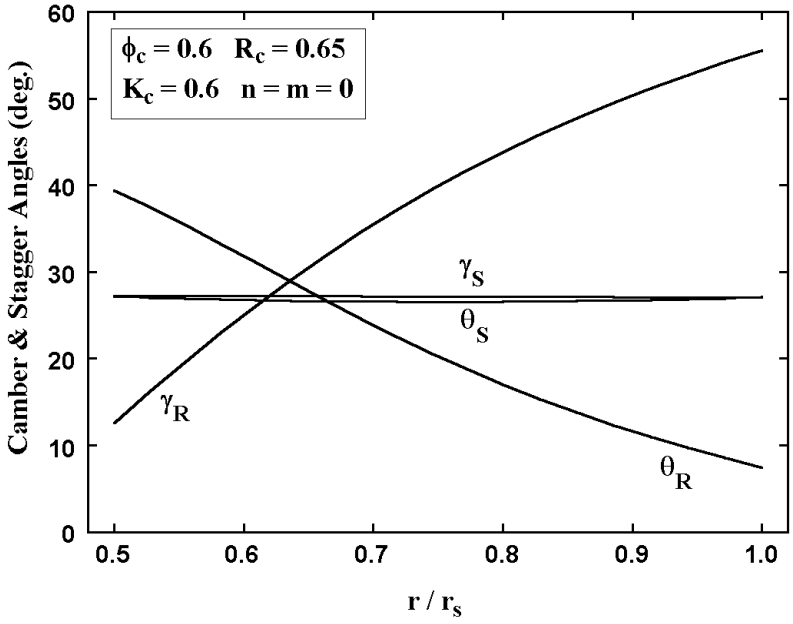

FIGURE 10-27 Constant Swirl Vortex Blade Angles

and stagger angles obtained using the blade design procedures of Section 10.3. In this case, NACA 65-series blades were designed with $t_b / c = 0.1$ and $\sigma = 1$ at $r = r_c$. The camber angles in Fig. 10-27 are the equivalent circular-arc camber angles defined in chapter 4. Note that the result is basically a constant-camber, constant-stagger stator blade. This is usually not too difficult to achieve. The constant swirl vortex style yields flow angles that essentially produce a linear variation of camber and stagger angle from hub to shroud. For any basic design parameters, constant camber is achievable by selecting the proper value of R_c, as illustrated in Fig. 10-25. By adjusting the other dimensionless performance parameters, the variation in stagger angle can usually be reduced to a point where constant stagger angles can also be used without significantly compromising performance. This would be a very cost-effective design for use as a standard repeating stage for industrial axial-flow compressors.

10.9 ASSIGNED FLOW ANGLE VORTEX FLOWS

Occasionally, it is useful to assign the absolute flow angle distribution at the rotor inlet or discharge rather than the swirl velocity distribution. Noting that $C_\theta = C_z \tan\beta$, it is easily shown that Eq. (10-24) can be replaced by

$$\frac{1}{C_z}\frac{\partial C_z}{\partial r} = -\frac{\cos^2\beta}{2r^2}\frac{\partial (r\tan\beta)^2}{\partial r} + \frac{\cos^2\beta}{C_z^2}\frac{\partial H}{\partial r} \tag{10-53}$$

The specification of ϕ_c, ψ_c and R_c defines β_{1c} and β_{2c}. If it is assumed that β varies linearly with r, and the difference between hub and shroud, $\beta_s - \beta_h$, is specified at either the rotor inlet or discharge station, Eq. (10-53) can be solved for the corresponding distribution of C_z. Since $C_\theta = C_z \tan\beta$, the swirl velocity distribution is also defined. For constant work stages, Eq. (10-21) defines the swirl distribution at the other station. This vortex specification is a useful variant on the constant swirl vortex type discussed in the previous section. Sometimes it is easier to fine-tune the blade angle distributions by refining the flow angle distribution rather than the swirl velocity distribution. Usually, it is more effective to specify the rotor exit flow angle distribution for this purpose. This vortex type can be quite useful, and it is easily incorporated into a computerized stage design system.

10.10 APPLICATION TO A PRACTICAL STAGE DESIGN

The stage design examples provided in the previous sections of this chapter have been rather arbitrary in illustrating some of the features of the various types of vortex flow styles. In practice, stage design is far more focused on specific design objectives and constraints. Usually there is substantial conflict between various desired design objectives in terms of establishing the specific stage design parameters.

In almost any axial-flow compressor design, minimum size, weight and cost will be important objectives. Clearly, these goals are best served by achieving a

large mass flow per unit frontal area, thus favoring a high flow coefficient stage. Similarly, reducing the number of stages required will be important, thus favoring a high work input coefficient design. As seen in Figs. 10-3 through 10-5, a high work input coefficient requires a high flow coefficient to avoid exceeding practical blade loading limits. So size, weight and cost considerations are definite incentives for the high flow coefficient and work input coefficient stages.

Good aerodynamic performance will also be an important objective for any axial-flow compressor design. Usually this is expressed in terms of efficiency and surge margin requirements. Surge margin may be expressed in terms of flow range or pressure-rise range between the design point and the surge limit. Surge margin and efficiency are not really independent concepts, although specific applications may impose special surge margin requirements. Normally, the stage design point is expected to be approximately its best operating condition. It is quite obvious that there is little merit in achieving optimum performance too close to the surge limit, where the stage will almost never operate in an actual compressor. In Section 10.2 it was shown that improved surge margin can be expected to favor low flow coefficients and low work input coefficients. In Figs. 10-7 through 10-9, Smith's (1958) recovery ratio parameter has strongly suggested that flow coefficients around 0.5 should be preferred. Smith (1958) seems to favor flow coefficient not exceeding 0.5 at any radius, although he notes that it may be difficult to achieve. Indeed, that seems a little impractical and perhaps not even desirable. Depending on the hub-to-shroud radius ratio, achieving a hub flow coefficient of 0.5 may require very low shroud flow coefficients. That may be as harmful as using flow coefficients that are too high, as can be seen in Fig. 10-7. Figs. 10-7 through 10-9 also show that low work coefficient (or K) is desirable and has the effect of reducing the significance of the flow coefficient selection.

The role of stage efficiency in setting stage design parameters is less significant than whether the surge margin is adequate to make use of the efficiency achieved. Indeed, if maximum efficiency is used as the major design criterion, the design point is very likely to be very close to the surge limit. This follows from the fact that designing for high work input may be the best way to reduce the impact of the losses on efficiency. Excellent stage efficiencies have been achieved for a wide range of stage performance parameters and vortex types. There is little credible evidence to associate any set of performance parameters or vortex type to optimum and practical design-point efficiency levels. It is sometimes suggested that optimum efficiency is associated with 50% reaction designs, although that is of questionable validity and of very little practical value. The stage reaction, in terms of R_c, will usually be established by surge margin considerations. Specifically, achieving satisfactory hub reaction and velocity ratios across the blades at the hub and shroud will usually be the major factors influencing the selection of R_c. Design approaches directed specifically toward increasing the stage design-point efficiency are generally beyond the scope of the methods described in this chapter. For example, special blade designs such as the controlled diffusion airfoils mentioned in Chapter 4, may be used. Some designers favor special features in the end-wall boundary layer regions, such as increased end-wall work. With modern viscous computational fluid dynamics codes, special designs to minimize secondary flow effects may be considered.

Clearly the designer is faced with conflicting priorities to trade off performance against size, weight and cost. Usually a parametric study will be required to select the best compromise, including evaluation of performance with the methods of Chapter 9. Unless carefully structured, such a parametric study can be very confusing and time-consuming. Usually the most efficient approach is to investigate alternate values of ϕ_c, while specifying the minimum acceptable values of the blade row velocity ratios, W_2/W_1 and C_3/C_2. Generally, the designer will be able to select an acceptable range of values for ϕ_c, while the minimum velocity ratios ensure reasonable blade loading and surge margin capability. Other constraints will be specified and monitored. For example, reasonable limits on flow angle, flow coefficient and work coefficient at all radii will normally be required. To illustrate the process, a simple optimization study has been conducted for the following constraints:

- $\phi_c = 0.5$
- W_2 / W_1 and $C_3 / C_2 \geq 0.73$
- β and $|\beta 1 < 70°$
- $\psi < 1$
- $\phi \leq 1$

Designs were generated for constant swirl vortex, free vortex and constant reaction vortex stages. The free vortex stage was not required to have $C_{\theta 1} = 0$ for this design. The design radius was chosen as the true mean stream surface, i.e., the root-mean-square average of the hub-and-shroud radii was used. The only parameters available to be selected are R_c and K_c (or ψ_c), which were chosen to best satisfy the constraints. In all cases, the velocity ratio across the stator proved to be controlling constraint, although the flow angle constraint was a significant factor for the constant reaction vortex. Figures 10-28 through 10-30 show the most important performance parameters to compare the three vortex types. It is seen that the free vortex design resulted in the highest rotor inlet relative velocities, making it the most susceptible to Mach number effects. The constant reaction vortex stage would appear to be the best choice for high Mach number applications, but that is a little misleading. That design is very close to the flow angle constraint near the shroud. It would be difficult to achieve adequate blade passage throat widths while using practical blade thicknesses, so blade passage choke could easily be a problem near the shroud. The constant reaction stage has the largest flow coefficient at the hub, but it is within the limit set for these sample designs. In other respects, the performance parameter distributions for the three designs are reasonably similar. Except for the rather large flow angles produced by the constant reaction vortex stage, the basic dimensionless performance and velocity triangle data provide little reason for preference of one design over the others.

The more significant differences in these three designs are seen in Figs. 10-31 and 10-32, which compare the blade geometry required for the three stage designs. In all cases, NACA 65-series blades were designed with constant chord, constant $t_b / c = 0.1$ and $\sigma = 1$ at $r = r_c$. All rotor blades are variable camber, twisted blades, but the constant reaction vortex stage requires the most extreme variations. Indeed, a negative camber angle is required at the shroud for that

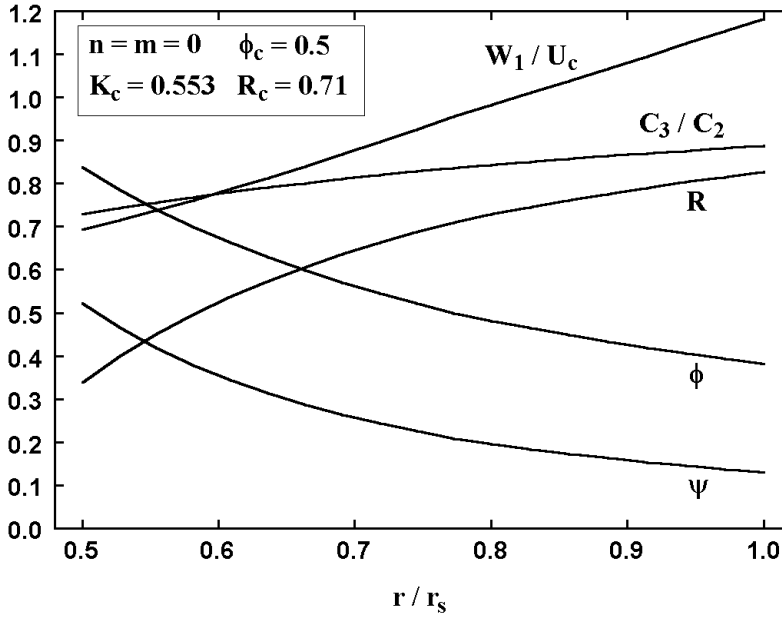

FIGURE 10-28 Constant Swirl Vortex Stage

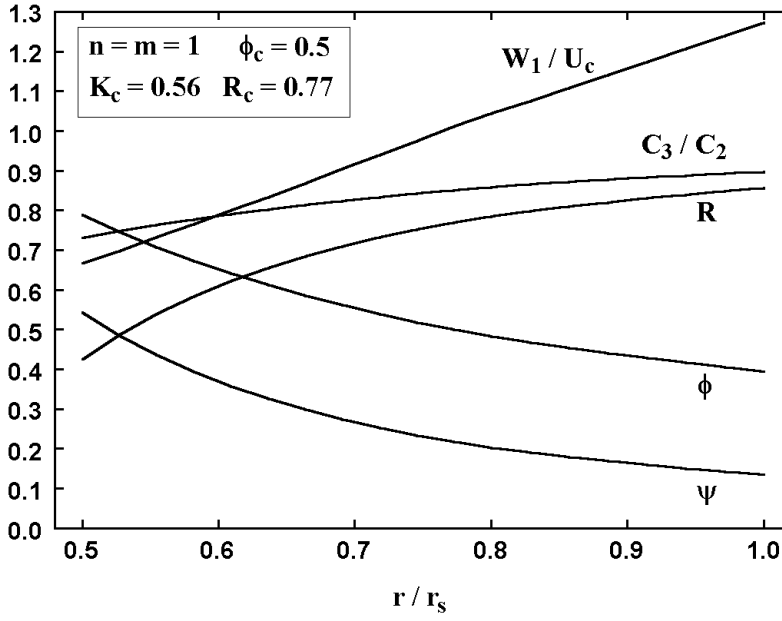

FIGURE 10-29 Free Vortex Stage

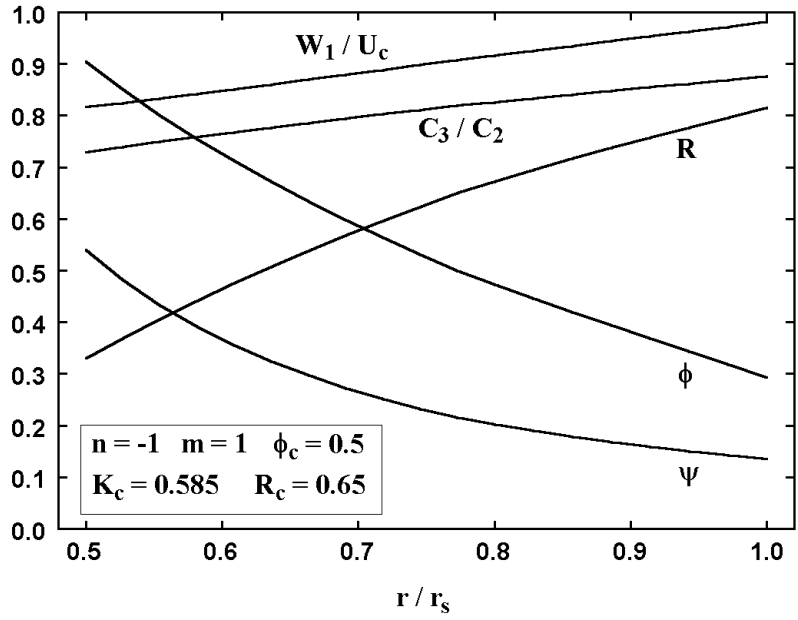

FIGURE 10-30 Constant Reaction Vortex Stage

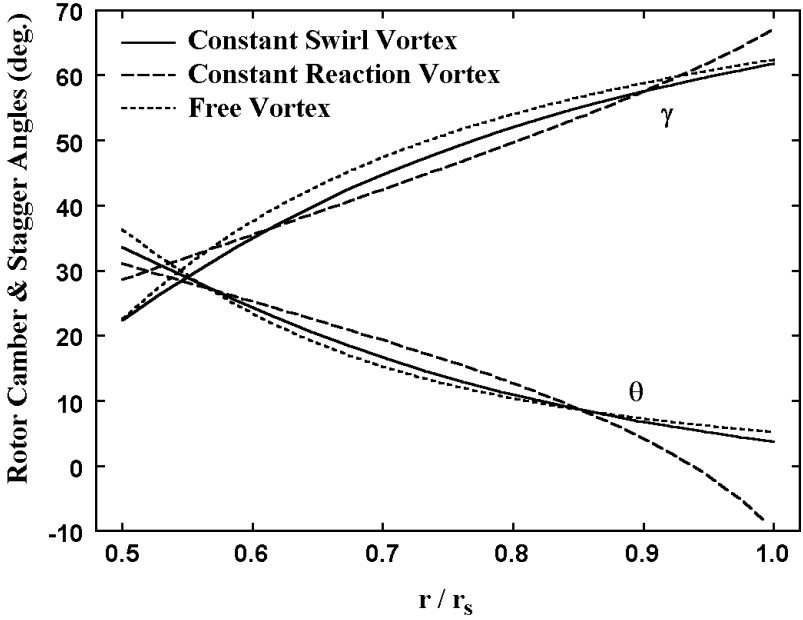

FIGURE 10-31 Rotor Blade Geometry

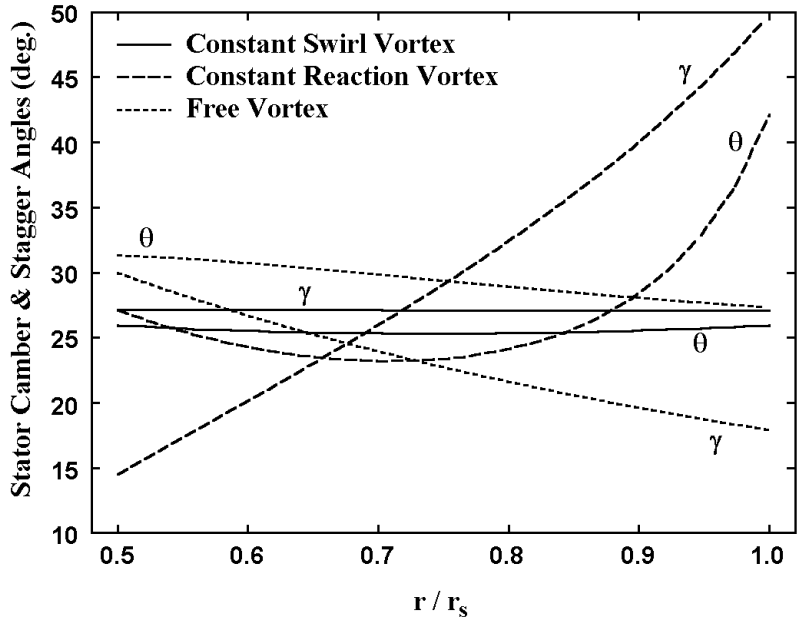

FIGURE 10-32 Stator Blade Geometry

design, with a very high stagger angle at the same location. The constant swirl vortex design results in very simple stator geometry, which is easily approximated by using constant camber and stagger angle blades. The free vortex stage requires variable camber, twisted stator blades, but with very reasonable variations. The constant reaction vortex stage requires highly twisted stator blades with a large variation in the camber angle. The constant reaction stage blades would need careful evaluation relative to its structural integrity and practicality for manufacturing. It is likely that application of this vortex style should be limited to higher hub-to-shroud radius ratios than those in this case

The performance analysis described in Chapter 9 was applied to these three stage designs to evaluate their expected performance. The annulus geometry for all stages was obtained by assuming a constant hub radius and sizing the shroud radius based on the same volume flow rate and rotation speed. This design volume flow rate is easily computed from the rotation speed and the free vortex velocity triangles, where C_z is constant. The rotation speed and inlet thermodynamic conditions were chosen to limit the maximum rotor inlet relative Mach number to about 0.78 to avoid biasing the comparison with Mach number effects. Once the approximate annulus sizing was accomplished, the shroud radii were adjusted to produce a conical shroud wall to avoid the results being biased by local contour angle variations that are not representative of a stage's true performance when used as a repeating stage in a multistage compressor. Similarly, end-wall boundary layer blockage and stream surface curvature

effects were ignored to obtain as fair a comparison as possible. This process produced the expected repeating stage for the free vortex and constant swirl vortex stage designs. That was not the case for the constant reaction vortex design, where a repeating stage configuration could not be achieved in practice. The annulus sizing to match the design velocity triangle for that case produced an increase in shroud radius across the rotor, followed by a large decrease across the stator. The most reasonable approximation to the annulus area schedule required was to simply assign a constant shroud radius. The source of the problem is the axial velocity ratios across the blade rows, which alter the predicted deviation angles as discussed in Chapter 6. As seen in Fig. 10-17, axial velocity ratios can be quite significant for this vortex style. The computerized stage design system used to generate these designs does not correct deviation angles for axial velocity ratio effects. To do so is usually misleading, since axial velocity ratios in an actual application may be quite different from those produced in the ideal stage design calculations. Application of a standard industrial compressor repeating stage involves use of various portions of the blade span in different stages as required to conserve mass flow rate. Adjustments in stagger angles and axial velocity levels through the multistage compressor are usually necessary to produce the required performance with a specific number of stages. If it is not possible to neglect the effect of axial velocity ratio on deviation angle in the basic stage design, the stage is simply not a good candidate for a standard repeating stage. That is really the case for this constant reaction vortex stage. The hub-to-shroud ratio used in this example is simply too low for a constant reaction vortex to produce a viable repeating stage. Of course, it is possible that this stage might be used in a single, specific application. In that case, the application-specific design procedures discussed in the next chapter should be used to design the blades for the stage.

Figure 10-33 presents a comparison of the performance predictions for the three stage designs. The lower limit of volume flow rate for each stage corresponds to the predicted stall limit based on stall criterion #3 of Chapter 9. It can be seen that the free vortex and constant swirl vortex stages produce essentially the same performance characteristics. The free vortex stage has a slight advantage in stable operating range, while the constant swirl vortex stage has a slight advantage in efficiency. Neither of these differences can be considered significant within the uncertainty of the performance analysis procedures. The constant reaction vortex design produces lower pressure ratios and efficiencies than the other two stages, even though it had the highest design work input coefficient, ψ_c. Based on the expected stage performance, either the free vortex or constant swirl vortex design could be selected. The simpler stator geometry of the constant swirl vortex stage and the higher rotor inlet relative Mach number level of the free vortex design would favor selection of the constant swirl vortex design.

10.11 A REPEATING STAGE AXIAL-FLOW COMPRESSOR

As mentioned at the beginning of this chapter, a repeating stage design can be used as a standard stage in industrial axial-flow compressors. Each industrial axial-flow compressor usually has a unique design. Pattern, tooling and development costs

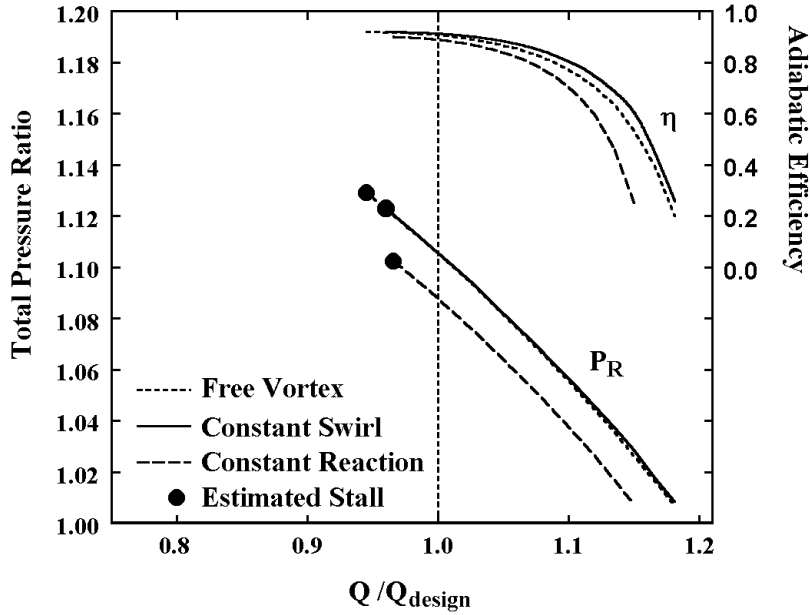

FIGURE 10-33 Comparison of Predicted Performance

are critical issues, since there are seldom any duplicate machines to share those costs. Similarly, experimental confirmation of the performance of the finished compressor will be obtained before it is shipped to the customer. Failure to achieve the guaranteed performance may require very expensive rework of the compressor. Use of a standard repeating stage can alleviate these problems. Now pattern and tooling costs can be shared among many industrial compressors, even though each one has a unique design. The risk of a performance deficiency is also greatly reduced, since experience with previous compressors can be used for guidance.

Application of a standard stage in a multistage compressor is reasonably straightforward using an aerodynamic performance analysis that is capable of sizing the annulus as described in Chapter 7. To illustrate the process, a ten-stage axial-flow compressor will be configured using the constant swirl vortex repeating stage designed in the previous section. The compressor will be designed with a constant hub radius, so that the same rotor blade can be used throughout, by simply trimming the blades to the proper shroud contour. Since constant-camber, constant-stagger stator blades can be used for the basic stage, a common stator blade is also usable. Under these constraints, it is easily seen that the basic blade geometry is identical for all stages. The simplest way to configure the basic compressor is to assign the mean stream surface meridional velocity through the compressor and size the annulus to define the approximate shroud contour. To simplify this process, the performance analysis is set up with one computing station between successive blade rows. Then the meridional velocity on the mean stream surface is assigned at specific computing stations and obtained at other

stations by linear interpolation with the station number. For this example, it will be assumed that the assigned meridional velocity must vary linearly with station number from the entrance to the first rotor to the exit of the last rotor. The compressor will be sized to use the full flow capacity of the standard stage, at the same rotation speed as that used in Fig. 10-33. So the meridional velocity at the entrance to the first rotor can be assigned immediately from the stage design data. Some fine-tuning is required to match the known shroud radius at this point due to the effect of gas density variations across the inlet guide vane and to the end-wall boundary layer blockage assumed at the compressor inlet. This requires a minor adjustment to the design inlet mass flow until the correct shroud radius is obtained. The sizing of the annulus for the entrance to the inlet guide vane and the exit to the last stator and the exit guide vane can be rather arbitrary at this point. As long as the meridional velocities assigned at these stations are not unreasonable, they have little influence on the performance. Manual sizing of the annulus at those stations is rather trivial once the shroud contour is defined at the other stations. So the task to be accomplished in this simple example is selection of the meridional velocity to be assigned at the last rotor exit. The first priority is to obtain a reasonable shroud contour. For example, assigning the meridional velocity on the mean stream surface to be constant through the compressor resulted in the shroud radius increasing with axial distance in the rear stages. This could be anticipated since the mean stream surface radius decreases through the machine. Since the axial velocity for the constant swirl vortex increases as the radius is reduced, it could be expected that the assigned meridional velocity should increase through the compressor. The assigned meridional velocity to be used at the last rotor discharge was easily determined by trial and error, using the performance analysis. Figure 10-34 shows the C_m distribution used and Figure 10-35 shows the hub-and-shroud contours developed by the annulus sizing with that C_m distribution. Figure 10-36 shows the predicted performance using the methods of Chapter 9. The estimated surge limit is also shown, including the stall criterion from Chapter 9 that was first encountered for each speed line. It can be seen that a standard repeating stage designed by the methods of this chapter can be effectively employed in a multistage compressor.

This application of a standard stage in a multistage compressor illustrates the conflicting priorities that the designer regularly encounters. The stage design in Section 10.10 followed practices expected to favor good efficiency and stable operating range. This was reasonably successful, but the cost-effectiveness of a ten-stage compressor that achieves a design pressure-ratio of about 2.2 is very questionable. The design constraints selected in Section 10.10 do not permit increasing the work coefficient to increase the pressure ratio. The compressor might be operated at a higher rotation speed to increase the pressure ratio, but only by exceeding the limit imposed on the rotor tip relative Mach number. It might be concluded that a standard repeating stage design is simply impractical for these design constraints. But that is really not the case. Rather, the stage hub-to-shroud radius ratio of 0.5 used throughout this chapter is not a good choice for an industrial axial-flow compressor using this as a standard repeating stage.

Figure 10-37 shows the important performance parameters for a constant-swirl vortex stage designed to the same constraints as for the design in Fig. 10-28, but with a hub-to-shroud radius ratio of 0.7. Note that a substantial increase in

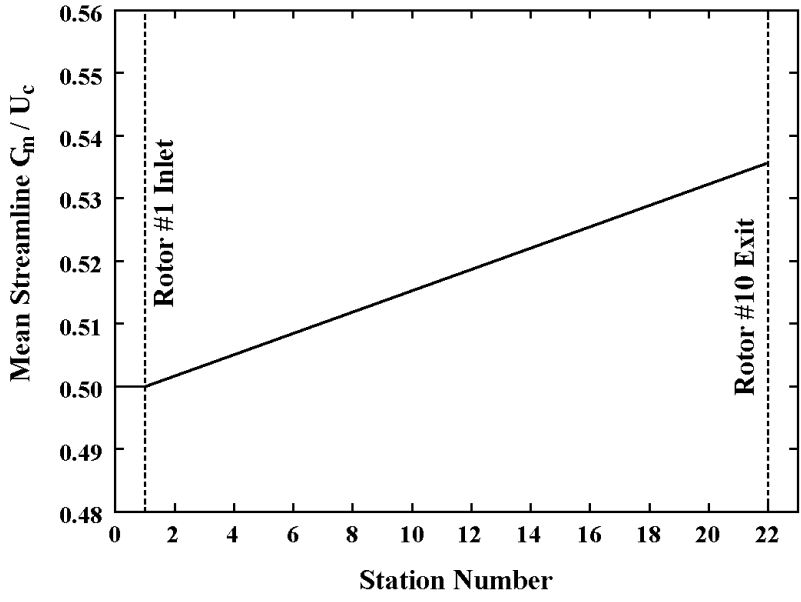

FIGURE 10-34 The Assigned C_m Distribution

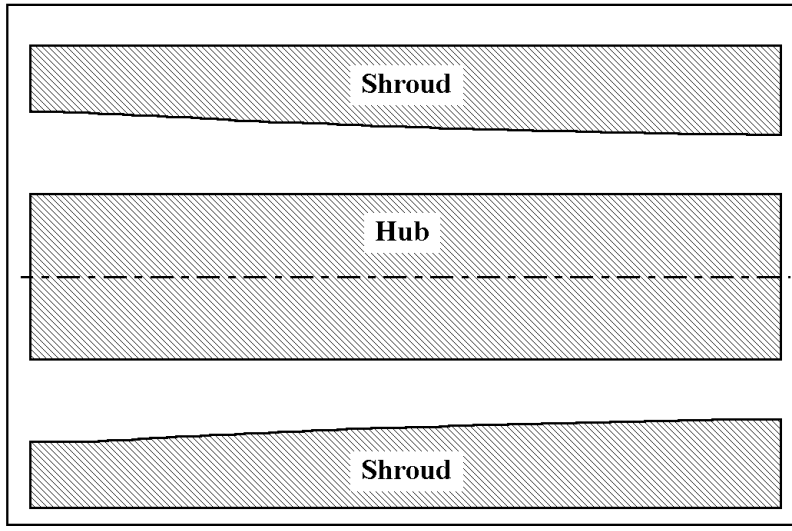

FIGURE 10-35 Hub-and-Shroud Contours

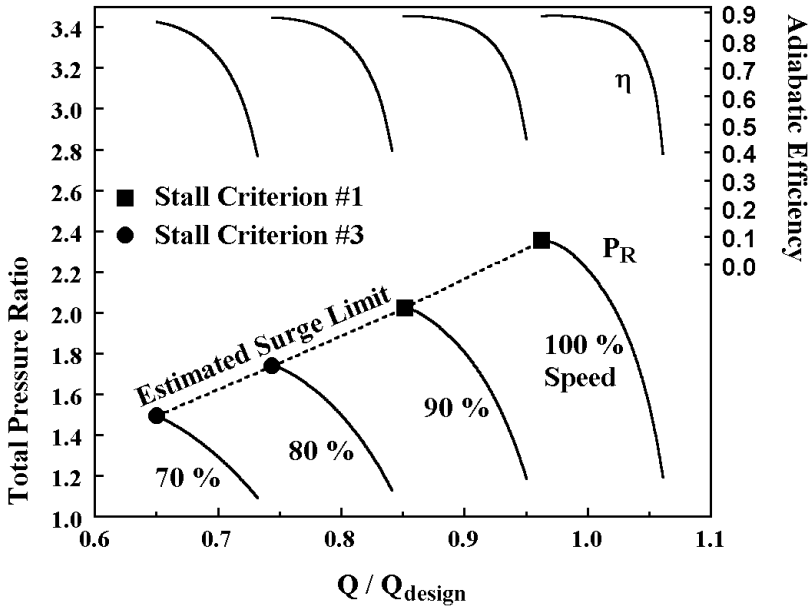

FIGURE 10-36 Aerodynamic Performance Prediction

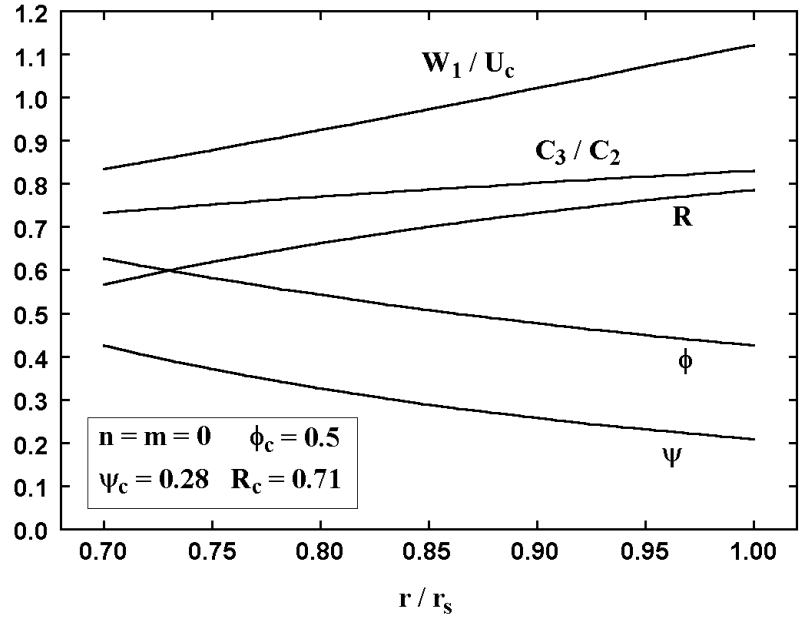

FIGURE 10-37 Alternate Constant-Swirl Vortex Stage

work coefficient is achieved while satisfying the same design constraints. An alternate 10-stage axial-flow compressor was configured using this alternate stage design as a standard repeating stage. This results in the predicted performance map shown in Fig. 10-38. This compressor achieves a pressure ratio of about 3.9 at the design mass flow rate. The larger hub-to-shroud radius ratio also results in higher efficiency for both the stage and the ten-stage compressor. Of course, the mass flow rate achieved is reduced relative to Fig. 10-36 due to the larger hub-to-shroud radius ratio. But scaling the geometry to a larger hub radius and reducing the rotation speed to obtain the desired mass flow rate, while maintaining the same dimensionless performance parameters and Mach number levels, could easily correct that.

In practice, application of a standard stage is more complicated than this simple illustration. It is unlikely that a direct application of the repeating stage will produce the design point flow and pressure ratio required. For example, it might be concluded that the application requires a $9^1/_2$-stage compressor with that configuration. In that case, it will be necessary to modify the design to achieve the required performance in either a 9-stage or a 10-stage compressor. This may require adjusting some of the blade stagger angles and modifying the C_m distribution. The stagger angle adjustment modifies the velocity triangles, while the C_m distribution can be used to expand or contract them. Both approaches can change the work input per stage to refine the overall pressure ratio to a more appropriate value. Both approaches will probably be needed to modify the performance while maintaining a good match between stages. After some experience with a specific

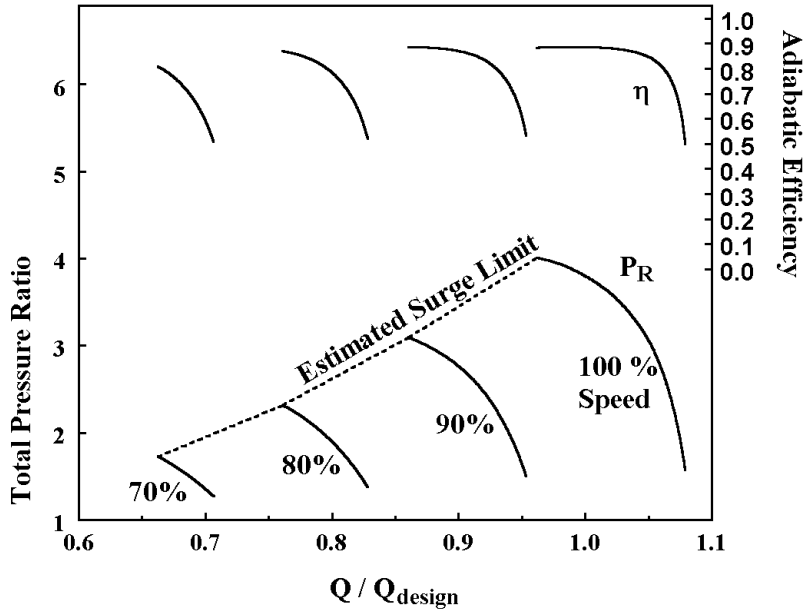

FIGURE 10-38 Alternate Compressor Performance

standard stage, the designer usually develops a fairly systematic approach to achieving the desired modifications. The same methods can be used to improve the surge margin, to better optimize the efficiency at a specific operating point of special interest, or even to achieve a flow capacity somewhat greater than the value for which the stage was designed. Hence, there is considerable flexibility when applying a standard stage, even though it was designed to be a simple repeating stage.

10.12 A COMPUTERIZED STAGE DESIGN SYSTEM

It is relatively simple to computerize the procedures described in this chapter into a systematic interactive design system. The most obvious use of this type of system is the design of standard industrial compressor stages such as those illustrated in the previous section. For that application, it is logical to ignore Mach number effects and losses, since they will vary with the specific application and the location of the stage in the multistage compressor. In Chapter 11, a more general approach is described where blades are designed specifically for each stage in a multistage compressor, including the effects of Mach number and losses. A computerized stage design system based on the methods from this chapter can be very useful to support that approach as well. It can provide a convenient method to investigate the alternate stage performance parameters and vortex types to be employed in the more general design approach. It can be rather cumbersome and confusing to attempt those investigations in the context of a multistage compressor design. Another application of a stage design system is for field-service repairs where a new stage design is required. This can occur if a stage is too damaged to determine its original geometry through reverse engineering. When a stage design system is available, it can often be a useful tool for a variety of simple and fast investigations to support other design activity. The effort required to develop a computerized system is so modest that it can be easily justified. It is advisable to include some additional flexibility, which is not covered in this chapter, when creating the computerized system. In particular, it is quite simple to provide for a variation of C_{zc} through the stage. Similarly, provision for a radial variation in work input is easily included for cases where additional end-wall work or imposed radial energy gradients are considered desirable.

EXERCISES

10.1 Show that Eq. (10-45) is valid for any constant-work, repeating stage.
10.2 Show that Eq. (10-48) is the condition to avoid reverse flow at the rotor exit for a constant reaction vortex flow in a constant-work, repeating stage.
10.3 Show that a constant-work, repeating stage can have constant reaction only for 100% reaction.